VISUAL DESIGN & ACADEMIC STUDIES COORDINATION OFFICE

Nabi SARIBAŞ - Hakan TERZİ - Nazan ÖZGÜR

PRINTED BY

Armoninuans Matbaa
Adres: Yukarıdudullu, Bostancı Yolu Cad. Keyap Çarşı B- 1 Blk. N.24 Ümraniye/İst.
Tel: 0216 540 36 11 pbx Faks: 0216 540 42 72 E-Mail: info@armoninuans.com

ISSN: 2146-0604

International Journal of Electronics, Mechanical and Mechatronics Engineering (IJEMME) is peer-reviewed journal which provides a platform for publication of original scientific research and applied practice studies. Positioned as a vehicle for academics and practitioners to share field research, the journal aims to appeal to both researchers and academicians.

Internationally indexed by EBSCO and DOAJ

CONTENTS

From Editor

Engineering Faculty of Istanbul Aydın University has started to publish an international journal on Electronics, Mechanical and Mechatronics Engineering, denoted as "International Journal of Electronics, Mechanical and Mechatronics Engineering (IJEMME)". We have especially selected the scientific areas which will cover future prospective engineering titles such as Robotics, Mechanics, Electronics, Telecommunications, Control systems, System Engineering, Biomedical, and renewable Energy Sources.

The manuscipt titled "PRODUCTION OF CLARITHROMYCIN LOADED CHITOSAN MICROSHERES BY SPRAY DRYING AN OPTIMIZATION STUDY " by Duygu ALTIOK dated year 2014, Volume 4, Number 1; is withdrawn.

We have selected only a few of the manuscripts to be published after a peer review process of many submitted studies. Editorial members aim to establish an international journal IJEMME, which will be welcomed by Engineering Index (EI) and Science Citation Index (SCI) in short period of time.

Prof. Dr. Zafer UTLU
Editor in Chief

Experimental Studies on Determination of Discharge Capacity of Circular Labyrinth Weirs Located on a Straight Channel

Omer BILHAN[1]
M. Emin EMIROGLU[2]

Abstract
Labyrinth weirs are particularly well suited for spillway rehabilitation where dam safety concerns, freeboard limitations, and a revised and larger probable maximum flow have required replacement or modification of the spillway. Labyrinth weirs with multiple crest elevations can be used in spillway design to confine base flows to a section of the crest and/or satisfy discharge hydrograph requirements. Labyrinth weirs provide higher discharge capacity than conventional weirs, with the ability to pass large flows at comparatively low heads. Over past 50 years many research investigations have considered the hydraulic performance of labyrinth weirs, particularly as dependent on the geometric features. The previous work has improved the design basis for such weirs. In the present study, discharge coefficients were experimentally determined for both sharp crested semi-circular labyrinth weirs and trapezoidal labyrinth weirs of side wall angle ($\alpha=37^0$). A comprehensive laboratory study including 9 models was conducted to determine the discharge coefficient of the semi-circular labyrinth weirs. It was found that from this experimental study the discharge coefficient of the circular labyrinth weir is higher than that of the linear weir, but lower than that of the trapezoidal weir.

Keywords: *Fluid Mechanics, Discharge Coefficient, Circular, Trapezoidal, Labyrinth Weir, Dam Safety*

1. Introduction

Generally a spillway consists of some type of control structure which is normally placed perpendicular to the flow direction. The capacity of spillway or a weir refers to the discharge for a given head of flow over its crest. Dams provide water supply (municipal, agricultural, industrial), flood control, hydropower, navigation, and recreation. Aging infrastructure, changes in land use, and higher peak flow predictions for extreme flood events often require upgrading or rehabilitating existing spillways. The replacement of linear weirs with nonlinear weirs (labyrinth weirs in many cases) is often considered as an alternative for increasing spillway discharge capacity without increasing the existing spillway channel width. Labyrinth weirs provide an effective means to increase the spillway discharge capacity of dams and are often considered for renovation projects required due to an

[1] *Nevsehir H.B.V. University, 5200, Nevsehir, Turkey, obilhan@nevsehir.edu.tr*
[2] *Firat University, 23100, Elazig, Turkey*

increase in expected flood inflow to the reservoir of an existing dam. Due to the complex design of the overflow structure, the labyrinth spillway discharge

capacity is affected by many factors including weir geometry and approach channel conditions [1]. A labyrinth weir is a linear weir that is 'folded' in plan-view to increase the crest length for a given channel or spillway width [2]. Figure 1 provides the key details of the labyrinth weir. For relatively small dams (<8 m high), it is often economical to construct a "full height" labyrinth, where the base slab is at the level of the embankment foundation. This construction eliminates the need for a chute to convey flow to the downstream toe and also simplifies the foundation design since the labyrinth structure is founded on natural soil as opposed to new compacted fill, which is more prone to settlement.

In general, labyrinth weir cycles follow a linear configuration; however, the discharge efficiency of the weir may be improved by orienting the cycles to the approaching flow. According to [3], the efficiency of Prado Spillway could have been increased by arcing the cycle configuration. Examples of curved or arced labyrinth spillways are: Avon [4], Kizilcapinar [5].

Optimizing the many geometric variables in the hydraulic design of a labyrinth weir can be challenging. For example, the sidewall angle (α), total crest length (L_c), crest shape, number of cycles (N), the configuration of the labyrinth cycles, and the orientation and placement of a labyrinth weir must all be determined. Furthermore, the geometry of a labyrinth weir causes complex 3-dimensional flow patterns that must be considered. The flow rate passing over the labyrinth is dependent on the crest length, which can be controlled by modifying the number of folds. The relationship between length and discharge is not linear, however, except for very small heads. As the water level above the labyrinth weir increases, four stages of nappe shape occur: fully aerated, partially aerated, transition and submerged. The thickness of nappe and depth of the tail water do not affect the discharge capacity of the labyrinth weir in the fully aerated flow condition. In this case, the labyrinth weir acts as a vertical cross section of the linear weir. As the water level above the labyrinth weir increases and the tail water rises, the nappe becomes partially aerated (adhering to the weir wall) and the discharge coefficient is reduced [5, 6].

Over the past 50 years, extensive research on the influence of geometric and hydraulic parameters on the hydraulic behavior of labyrinth weirs, particularly on the discharge capacity, has been completed. In [7], presented initial studies on the behavior of labyrinth weirs and presented the hydraulic performance as it compares with that of sharp-crested weirs. In [8], followed up on Taylor's work and developed design criteria for labyrinth weirs. Based on their research findings, they suggested Eq. (1) for the discharge coefficient of labyrinth weirs.

$$C_d = 3.22 + 0.40 \, h/P \tag{1}$$

where C_d is the discharge coefficient, h is the depth of flow over the weir crest and P is the weir height.

Additional work in [4] utilized the results from physical model studies to expand on the theory and develop a family of curves to evaluate spillway performance. Extensive physical model studies were performed in [9] to evaluate various labyrinth geometries and approach conditions. The U.S. Bureau of

Reclamation (USBR) tested a model of labyrinth spillway for Ute Dam and Hyrum Dam [9, 10]. They found that the discrepancy between their observations and those were caused by difference in head definition [8].

Case studies for Boardman Dam [11] and Hyrum Dam [10] reported that curved abutment walls upstream of the labyrinth weir minimized the loss of efficiency caused by flow separation. The test program for a 2-cycle labyrinth weir for Hyrum Reservoir in [10] included various weir orientations and placements (Normal, Inverse, Flush, and Partially Projecting). For similar entrance conditions, it was reported that the Partially Projecting orientation increased discharge by 10.4% when compared to the Flush orientation and the Normal orientation had a 3.5% greater discharge than the Inverted orientation [12].

In [13], has investigated model studies of the labyrinth weir and Eq. (2) is his suggested equation for calculation of discharge over labyrinth weirs.

$$Q = C_d \left(\frac{\frac{Wc}{P}}{\frac{Wc}{P+K}} \right) W_c H_t \sqrt{g H_t} \qquad (2)$$

where Q is the discharge over labyrinth weir, C_d is the discharge coefficient, H_t is the total upstream head measured relative to the weir crest, W_c is the channel width and P is the weir height.

In [14], calculated discharge coefficient (C_d) of labyrinth weirs as function of L/w and H_t/P parameters. They defined discharge capacity of labyrinth weirs with Eq. (3).

$$Q = C_d W_T 2 g H_t^{1.5} \qquad (3)$$

In [15], carried out extensive experimental work on the performance of the labyrinth weir. They proposed a flow equation for the labyrinth weir that is identical to the basic equation applicable to a linear weir, but with modification of the coefficient of discharge. They also presented experimental data of the variation of discharge coefficient of labyrinth weir with a head to weir height ratio (H_t/P) for side wall angles (α) of 6° to 18°. Additional curves for weir side angles of 25° and 35° were obtained by extrapolation. In [16], extended this work by providing a dimensionless head-discharge relationship for submerged labyrinth weirs. Using a physical model of the labyrinth weir of Dog River Dam in Georgia, [17] showed that the method produced a discharge error up to ± 25% [15].

Labyrinth weirs are also used as side weirs to increase the outflowing discharge. In [18] and [19] carried out extensive experimental work on the performance of the labyrinth side weirs and presented coefficient of discharge curves in a simplified way as compared to previous investigators. Further work on triangular labyrinth side weirs was completed by [20] using Artificial Neural Network (ANN) techniques to calculate the discharge coefficient under critical flow conditions.

In [18], studied the discharge coefficient of a semi-elliptical side weir in subcritical flow on a straight channel. The authors presented the discharge coefficient of the semi-elliptical side weir which is higher than that of the rectangular side weir, but lower than that of the triangular labyrinth side weir.

In [21], carried out flume studies on trapezoidal labyrinth weirs for side wall angles 6°, 8°, 10°, 16°, 21°, 26° and 30°. In [22], extended these studies for a wider range of flow conditions.

In [23], used laboratory-scale physical models to compare the hydraulic efficiency of the Piano Key (PK) weir design with that of a geometrically similar rectangular labyrinth weir, with and without sloping floors installed in the inlet and outlet keys. The test data showed that the PK weir was more efficient than the geometrically comparable rectangular labyrinth weir, a fact likely attributable to a reduction in entrance losses associated with the PK weir inlet key geometry.

In [24], studied the outflow process from a sharp-crested triangular labyrinth weir. Applying dimensional analysis and the Π theorem, five dimensionless parameters were determined as important to the description of the outflow process. A dimensionless stage-discharge relation was developed.

In [25], published labyrinth weir design equations that are applicable to in-channel labyrinth weir applications in which the approach flow is oriented normal to the weir carried axis. Consequently, some uncertainty exists regarding the hydraulic performance of labyrinth weir configurations that deviate from the experimental conditions associated with the empirical determinations.

In [26], investigated the labyrinth weir nappe interference and identified labyrinth weir flow characteristics that decrease discharge efficiency, including local submergence. The authors presented parametric methods for quantifying nappe interference region size as a function of weir geometry (e.g., sidewall angle and crest shape) and flow conditions (e.g., headwater and nappe aeration).

While all these documented studies have provided significant insights to the behavior of labyrinth weirs under specific conditions, the general theory remains: the capacity of labyrinth weir is a function of the upstream total head, the effective crest length, and the coefficient of discharge. The discharge coefficient depends on the total head, weir height, thickness, crest shape, apex configuration, and angle of side wall. While viscosity and surface tension are also significant variables, their influence is limited at velocities of sufficient magnitude and by appropriate model geometries [23].

The purpose of this study is to systematically investigate the discharge capacity of sharp-crested circular labyrinth weir, using a broad range of experiments, and considered together with the other effective dimensionless parameters.

2. Experimental Set-up and Experiments

Semi-circular labyrinth weir experiments were conducted at the Hydraulic Laboratory of Firat University, Elazig, Turkey. Experiments were conducted at stable flow conditions and free overflow conditions. The experimental set-up includes sump, pumping system, discharge tank, rectangular flume, digital flowmeter and labyrinth weir (Fig. 1). Water is recirculated through 250 mm diameter of supply line using two 75 HP pumps. Water for experimental setup is taken from the supply line by means of a pipe with 150 mm diameter. The discharge was measured by means of a Siemens electromagnetic flow-meter installed in the supply line. Water was supplied to the main channel (2 m wide and 0.80 m height this channel length is 3.0 m) through a supply pipe from the sump (volume of 15 m^3) with flow controlled by a gate valve. For damping the water surface waves and reducing turbulence, baffle wall and wood surface dampener is provided. In the experiments, the upstream elevation was built higher than the downstream elevation so that free flow conditions occur downstream of the weir.

Sheet metal materials which have 4 mm thickness (t) were used for labyrinth weirs. Labyrinth weirs designed as three- cycles. Schematic view of circular labyrinth weir is given in Fig. (2). Each semi-circular labyrinth weir and linear weir models with a sharp crested shape was tested in the experiments (Examples shown in Fig. 3).

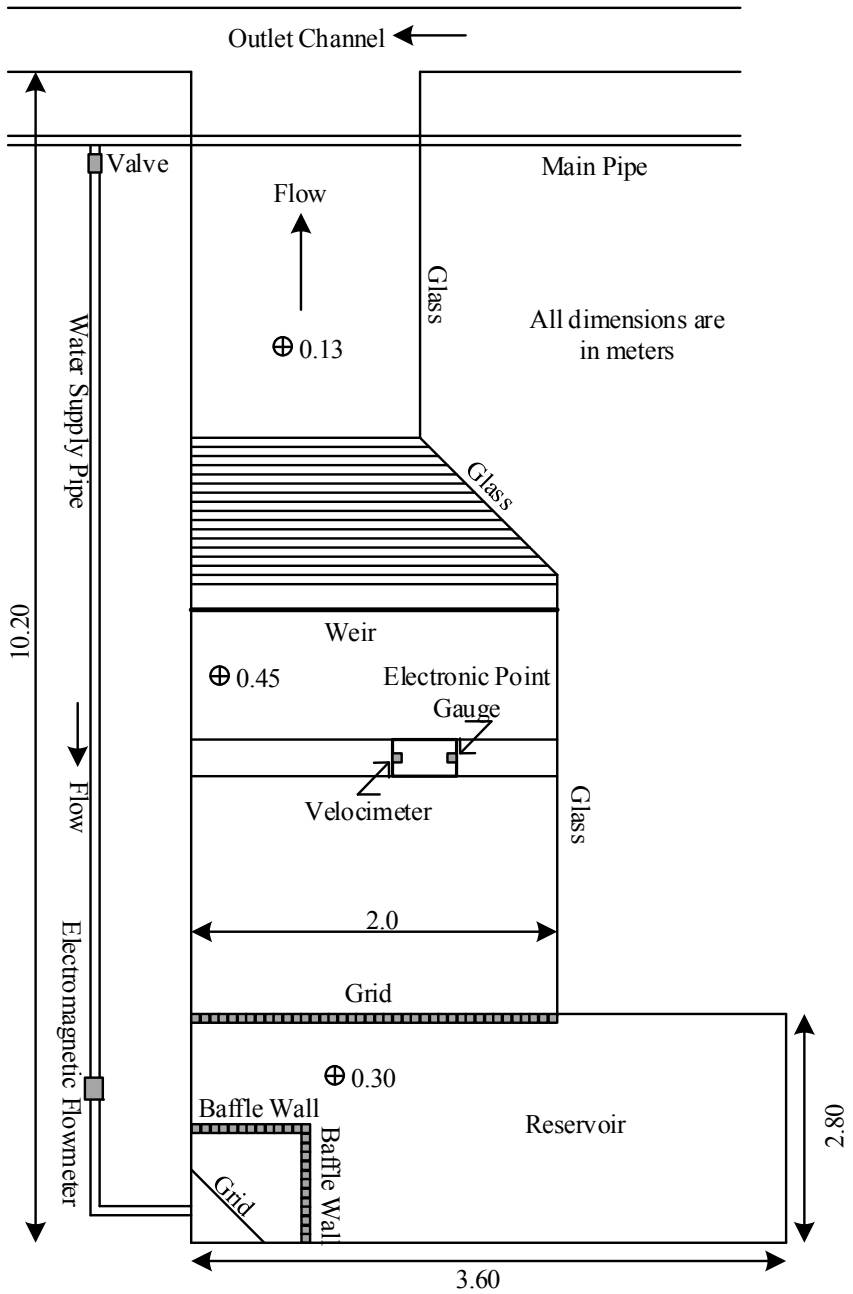

Fig. 1 Experimental arrangement

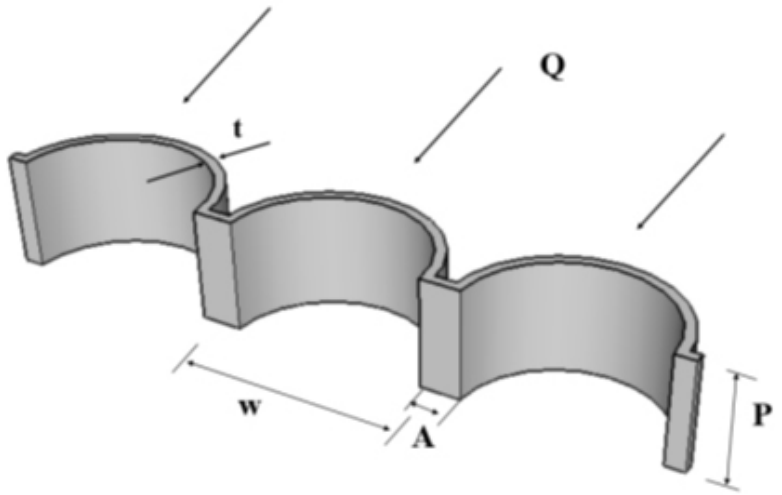

Fig. 2 Schematic view of the circular labyrinth weirs located on straight channel

Circular Labyrinth Weir Linear Weir

Fig. 3 Experimental set-up for circular labyrinth weir and linear weir

To measure the nappe height, water depth was measured accurately using Mitutoyo digital point gauges (accurate to ±0.01 mm) just upstream of the weirs. Level measurements were taken at a distance from the weir equal to five times the nappe height. For flow rate measurements, Nortek brand acoustic three-axis velocimeter was used.

In the experiments, the weir heights were taken as 100 mm, 150 mm and 200 mm and apex width (A) was taken as 80 mm. Sharp-crested shapes is provided for all models. All experiments were performed according to free flow conditions.

The flow over labyrinth weir is three dimensional and does not readily fit into mathematical description and hence the discharge function is found through experimental studies and analysis. The crest coefficient depends on the total head, weir height, thickness, crest shape, apex configuration and angle of side wall. To

simplify the analysis, the effect of viscosity and surface tension could be neglected by selecting model and velocity of sufficient magnitude.

The discharge over labyrinth weir can be expressed as:

$$Q = \frac{2}{3} C_d \sqrt{2g} H_t^{1.5} L \qquad (4)$$

where Q is the discharge over a labyrinth weir; C_d is the discharge coefficient of the labyrinth weir; L is the effective length of labyrinth weir; H_t is the total head ($V_0^2/2g + h$) and g is the gravitational acceleration constant (Fig 4).

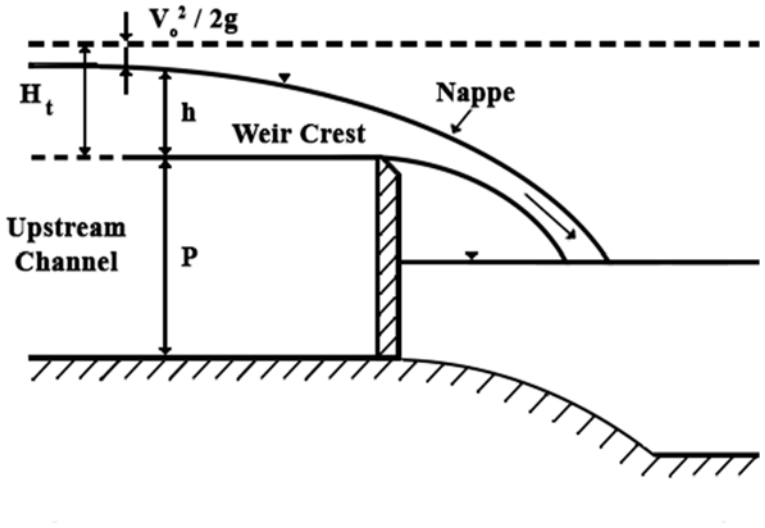

Fig. 4 Definition sketch for flow over a sharp crested weir

Head over labyrinth weir was measured for different value of discharges in the range of 14.7 L/s to 136.9 L/s. In this range, the head over the labyrinth weir varied from 10 to 90 mm. The models of linear weir a trapezoidal labyrinth weirs are also tested in the same Flume for the purpose of comparison. In the experiments, the characteristics of the circular labyrinth weirs, trapezoidal labyrinth weirs and linear weirs which are tested in the experiments are given in Table 1.

Table 1. Physical model geometrics for labyrinth weirs tested in the present study

Models	W_c (cm)	P (cm)	L (cm)	N	A (cm)	L_c / w	Type of Weir
1	196	10	196	-	-	-	Linear Weir, α=90°
2	196	15	196	-	-	-	Linear Weir, α=90°
3	196	20	196	-	-	-	Linear Weir, α=90°
4	196	10	294	3	8	1.50	Circular Labyrinth Weir
5	196	15	294	3	8	1.50	Circular Labyrinth Weir
6	196	20	294	3	8	1.50	Circular Labyrinth Weir
7	196	10	294	3	8	1.50	Trapezoidal Labyrinth Weir, α=37°
8	196	15	294	3	8	1.50	Trapezoidal Labyrinth Weir, α=37°
9	196	20	294	3	8	1.50	Trapezoidal Labyrinth Weir, α=37°

3. Experimental Results and Analysis

Experiments are carried out on three circular labyrinth weir models, and three linear weir models having sharp crested shape similar to labyrinth weirs models. Moreover, the results of the present study compared well with trapezoidal labyrinth weirs and linear weirs as shown in Fig. 5 and Fig. 6. On all these models, head-discharge measurements are taken for weir height of P=10, 15 and 20 cm. A total of 9 different configurations were examined in these experiments.

Discharge coefficient for labyrinth weirs was computed using equation (Eq. (4). Discharge coefficients of circular labyrinth side weirs have much higher values than the conventional weirs. The effect of crest shape on the discharge coefficient is very significant for the same channel width and crest length.

When the weir is placed at an acute angle to the flow, the flow becomes three dimensional. For linear weirs, all the streamlines are perpendicular to the crest and are two-dimensional. But for inclined weir, like a labyrinth weir, the streamlines under the nappe are almost perpendicular to the crest, whereas at the free water surface the streamlines are pointing towards the downstream direction. The labyrinth weir flow becomes further complicated due to interference of jets near the upstream apex of the labyrinth. At high discharges, the jets from adjacent crests strike each other and in the process create a nappe that is not aerated. This results in decrease of discharge coefficient of the labyrinth weirs.

From the present experiments results, the variation of C_d for circular labyrinth weirs with H_t/P is plotted for P=10, 15 and 20 cm in Fig.5. It is noted that discharge coefficient for labyrinth weirs is computed using equation (Eq. (4)). It is apparent from the results in Fig. 5 and Fig. 6 that discharge capacity of the labyrinth weirs is much higher than the conventional weirs. The primary reason for this is that the crest length of the labyrinth weir is much longer than that of the conventional weir.

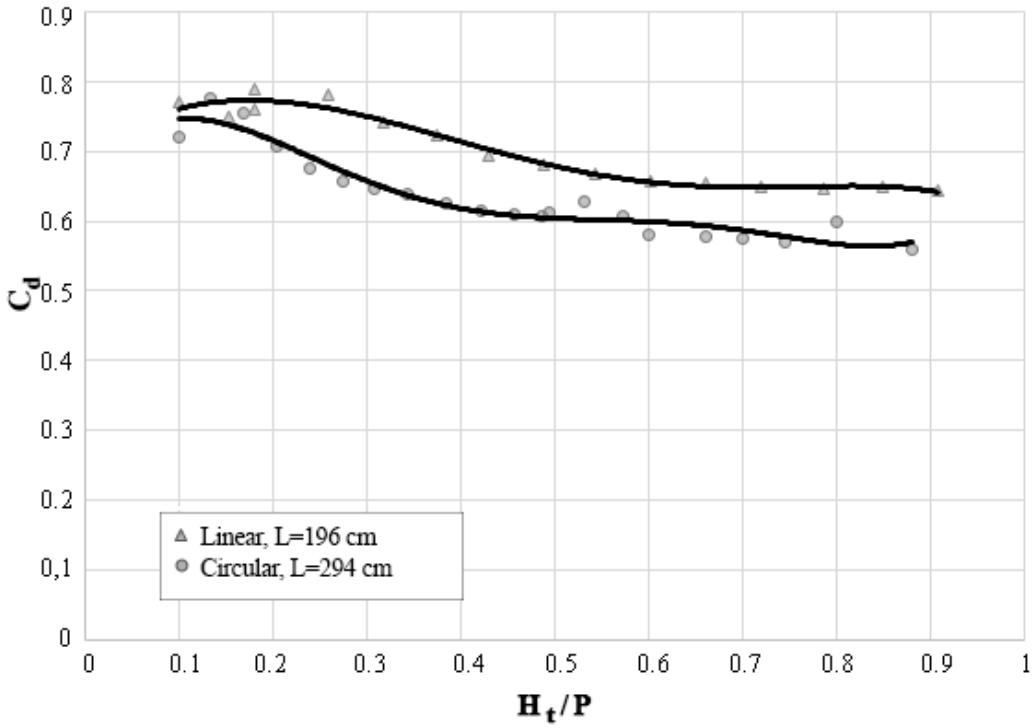

Fig. 5 Variation of discharge coefficient (C_d) with Head to weir height (H_t/P) for circular and linear weirs

Also, the variation of discharge coefficient (C_d) with head to weir height (H_t/P) for trapezoidal labyrinth weir (α=37°, L=294 cm, N=3, P=10-15-20 cm) and circular labyrinth weir (L=294 cm, N=3, P=10-15-20 cm) which have the same crest length is plotted in Fig. 6.

The discharge capacity of trapezoidal labyrinth weir according to the circular labyrinth weir can be seen to be higher in Fig. 6. This results especially can be seen in the H_t/P values between 0.1 to 0.6.

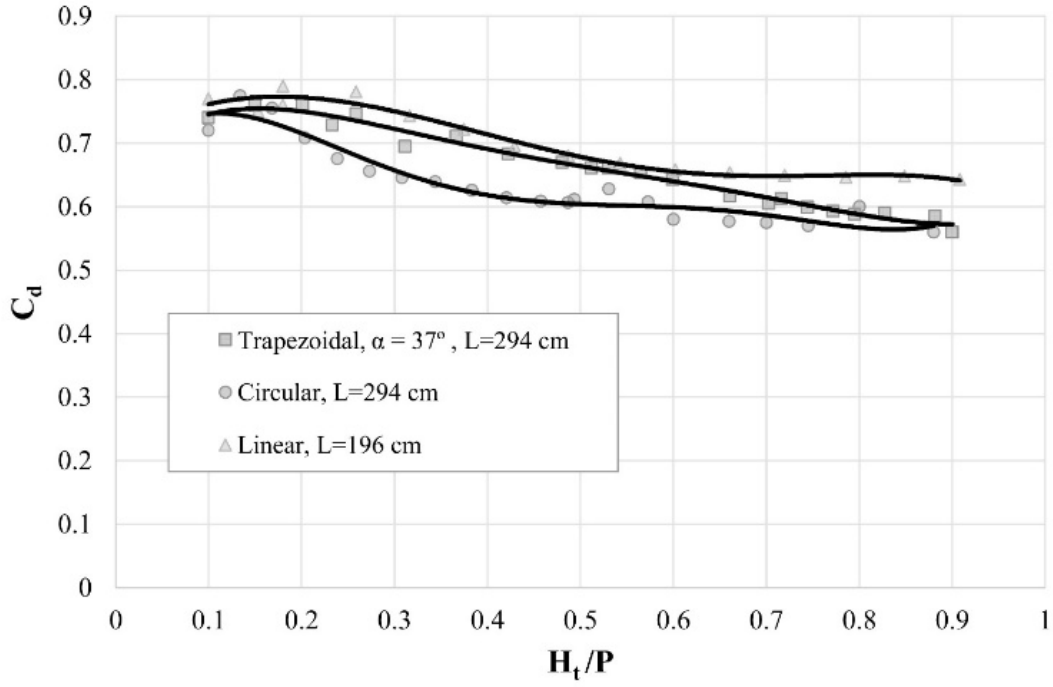

Fig. 6 Variation of discharge coefficient (C_d) with head to weir height (H_t/P) for trapezoidal, circular labyrinth weirs and linear weir

In Fig. 6, the sudden decrease in weir efficiency varies (caused by the weirs shifting out of the clinging nappe aeration regime) but is present for all tested sharp-crested weirs in the range from 0.3 to 0.5 of H_t/P.

To represent the data of the equation form, correlation analysis is carried out for the observed data for each model, separately. The 5th degree polynomial provides a reasonable fit between C_d and H_t/P. Thus, discharge coefficient (C_d) of sharp-crested labyrinth weir is expressed as:

$$C_d = A_0 + A_1\left(\frac{H_t}{P}\right) + A_2\left(\frac{H_t}{P}\right)^2 + A_3\left(\frac{H_t}{P}\right)^3 + A_4\left(\frac{H_t}{P}\right)^4 + A_5\left(\frac{H_t}{P}\right)^5 \quad (5)$$

The values of C_d for circular labyrinth weirs and linear weirs, A_0 to A_5 and R^2 are shown in Table 2.

Table 2. Coefficient of discharge per unit length of circular labyrinth weirs

Model	A_0	A_1	A_2	A_3	A_4	A_5	R^2
Circular	0.6416	2.2646	-3.4166	38.676	-1.8340	16.310	0.9239
Linear	0.6991	0.9370	15.683	2.4939	41.490	-1.9528	0.9665

4. Conclusions

Labyrinth weirs provide an effective means to increase the spillway discharge capacity of dams and are often considered for renovation projects required due to an increase in expected flood inflow to the reservoir of an existing dam. The hydraulic performance of traditional labyrinth weirs is well known since they have been studied for a long time. Nevertheless, analytical design equations considering all the involved parameters are not yet available. The design has to be based on experimentally derived and generalized performance curves.

According to this experimental study, it was found that the trapezoidal labyrinth weirs are hydraulically more efficient than the circular labyrinth weirs and linear weirs from the perspective of ease of construction and the discharge capacity.

The values for discharge coefficient of circular labyrinth weir and linear weir can be suitably obtained from the design curves and the regression equations generated through this study.

Of course, given unlimited width, greater efficiencies (discharge per head) will be obtained for a linear weir. However, the trapezoidal labyrinth weirs provides much greater weir length in confined space with only limited reductions in efficiency (reduction in C_d). The circular weir is the least efficient of those investigated.

It was found that the discharge coefficient of circular labyrinth weir C_d increases when the L ratio and number of labyrinth weir cycles (N) increases. The discharge coefficient of the circular labyrinth weir is higher than that of the linear weir, but lower than that of the trapezoidal weir.

It is recommended that a labyrinth weir design be verified with a physical or numerical model study, as it would include site-specific conditions that may be outside the scope of this study and may provide valuable insights into the performance and operation of the labyrinth weir.

Variation of the nappe pressure between sub-atmospheric pressure and atmospheric pressure causes vibrations, oscillations and noise. Although the negative pressures under water nappe partially increase the discharge capacity of the labyrinth weirs, effects of vibration and resonance may cause problems that could threaten the safety of the structure.

The authors are continuing research using nappe breakers to model non-standard labyrinth geometries and approach conditions

for increasing discharge capacity of labyrinth weirs.

Acknowledgment
Funding for this study was provided by the Scientific Research Project Department of Firat University in Turkey, Project No: 1610.

NOTATION

A Apex width;
C_d Discharge coefficient;
g Acceleration constant of gravity;
h Depth of flow over the weir crest;
H_t Total upstream head measured relative to the weir crest;
H_t/P Headwater ratio;
N Number of labyrinth weir cycles;
P Weir height;
Q Discharge over weir;
V Average cross-sectional flow velocity stream of weir;
W_c Channel width;
w Width of a single labyrinth weir cycle;
L Total crest length of labyrinth weir;
L_c Total crest length for a single labyrinth weir cycle;
R^2 Determination coefficient;
t Weir wall thickness.

REFERENCES

[1] Yıldız D., Uzucek E. (1993) Labirent dolusavakların projelendirilme kriterleri. Devlet Su İşleri Teknik Araştırma Kalite ve Kontrol Dairesi Başkanlığı. Yayın No: HI-862 Ankara.
[2] Crookston, B. M., and Tullis, B. P. (2012c) Labyrinth weirs: Nappe interference and local submergence. J. Irrig. Drain. Eng., 138(8), 757–765.
[3] Falvey, H.T., (2003) Hydraulic Design of Labyrinth Weirs. ASCE Press, 162p.
[4] Darvas, L. (1971) Discussion of performance and design of labyrinth weirs, by Hay and Taylor. J. Hydraul. Eng., ASCE, 97(80), 1246–1251.
[5] Yıldız, D., Uzucek, E. (1996) Modeling the performance of labyrinth spillways. Int. J. Hydropower Dams, 3, 71–76.
[6] Tsang, C. (1987) Hydraulic and aeration performance of labyrinth weirs. Ph.D. dissertation, University of London, London.
[7] Taylor, G. (1968). The performance of labyrinth weirs. PhD thesis, University of Nottingham, U.K.
[8] Hay, N., and Taylor, G. (1970) Performance and design of labyrinth weir. J. Hydraul. Eng., 96(11), 2337–2357.
[9] Houston, K. (1982) Hydraulic model study of Ute dam labyrinth spillway. Rep. No. GR-82-7, U.S. Bureau of Reclamation, Denver.
[10] Houston, K. (1983) Hydraulic model study of Hyrum dam auxiliary labyrinth spillway. Rep. No. GR-82-13, U.S. Bureau of Reclamation, Denver.
[11] Babb, A. (1976). "Hydraulic model study of the Boardman Reservoir Spillway." R.L Albrook Hydraulic Laboratory, Washington State University, Pullman, Wash.
[12] Crookston, B. M., and Tullis, B. P. (2011) "The design and analysis of labyrinth weirs" 31st Annual USSD Conference. San Diego, California, April 11-15, Pages: 1667-1681.
[13] Lux, F., (1989) Design and Application of Labyrinth Weirs, Design of Hydraulic Structures 89, Balkema, Rotterdam, ISBN, 90, 6191 – 8987.
[14] Magalhaes, A., and Lorena, M. (1989) Hydraulic design of labyrinth weirs. Rep. No. 736, National Laboratory of Civil Engineering, Lisbon, Portugal.

[15] Tullis, B. P., Amanian, N., and Waldron, D. (1995) Design of labyrinth weir spillways. J. Hydraul. Eng., ASCE, 121(3), 247–255.

[16] Tullis, B. P., Young, J., and Chandler, M. (2007) Head-discharge relationships for submerged labyrinth weirs. J. of Hydraul. Eng., ASCE, 133(3), 248–254.

[17] Savage, B., Frizell, K., and Crowder, J. (2004) "Brains versus brawn: The changing world of hydraulic model studies". ASDSO 2004 Annual Conf. Proc., Association of State Dam Safety Officials (ASDSO), Lexington, KY. May, 4. ⟨www.usbr.gov/pmts/hydraulics_lab/pubs/PAP/PAP-0933.pdf⟩.

[18] Emiroglu, M. E., Kaya, N., and Agaccioglu, H. (2009)."Discharge capacity of labyrinth side weir located on a straight channel."J. Irrig. Drain. Eng., ASCE, 136(1), 37–46.

[19] Kaya, N., Emiroglu, M. E., and Agaccioglu, H., (2011) "Discharge coefficient of a semi-elliptical side weir in subcritical flow." Flow Measurement and Instrumentation, Volume: 22, 25-32.

[20] Bilhan, O, Emiroglu, M. E., Kisi, O, (2011) Use of artificial neural networks for prediction of discharge coefficient of triangular labyrinth side weir in curved channels. J. Advances in Eng. Soft. 42(4), 208-214.

[21] Khode, B.V., Tembhurkar, A.R. Porey, P.D. and Ingle R.N. (2011) Determination of Crest Coefficient for Flow over Trapezoidal Labyrinth Weir. World Applied Sciences Journal 12 (3): 324-329.

[22] Khode, B. V., Tembhurkar, A. R. P. D. Porey and R. N. Ingle, (2012) Experimental Studies on Flow over Labyrinth Weir. Journal of Irrig. Drain Eng. ASCE, 138:548-552.

[23] Anderson, R. M. and Tullis, B. P., (2012) Comparison of Piano Key and Rectangular Labyrinth Weir Hydraulics. J. Hydraul. Eng. 138:358-361.

[24] Carollo, F., Ferro, V., and Pampalone, V. (2012). Experimental Investigation of the Outflow Process over a Triangular Labyrinth-Weir. J. Irrig. Drain Eng., 138(1), 73–79.

[25] Crookston, B. M., and Tullis, B. P. (2012a) Arced labyrinth weirs. J. Hydraul. Eng., 138(6), 555–562.

[26] Crookston, B. M., and Tullis, B. P. (2012b) Discharge efficiency of reservoir-application-specific labyrinth weirs. J. Irrig. Drain. Eng., ASCE, 138(6), 773–776.

A Prediction Model for Performance Analysis in Wireless Mesh Networks

Safak Durukan ODABASI[1]
Ergun GUMUS[2]

Abstract
Analysis of computer networks is an important study field that must be handled carefully in order to make communication systems work properly. Efficient evaluation and remodelling of system according to factors affecting the performance is required. For this aim, many techniques have been proposed, so far. However, machine learning methods are getting more preferable than others with their cost-effective and faster solutions. In this study, generalized regression neural networks (GRNNs) approach was employed in order to predict the output, packets dropped of a sample DMesh network simulation. The simulation is driven by parameters such as number of nodes, number of gateways, number of channels used, and traffic density. It was observed that parameters: traffic density and number of channels used, have a direct impact on error rate of the regression model. The high variance explained values show that GRNN approach can represent real characteristics of DMesh architecture.

Keywords: *Mesh Networks, Source Management, Prediction Model, Generalized Regression Neural Networks, Performance Analysis*

[1] *Department of Computer Engineering, Istanbul University, 34320, Avcilar, Istanbul, Turkey, sdurukan@istanbul.edu.tr*
[2] *Department of Computer Engineering, Istanbul University, 34320, Avcilar, Istanbul, Turkey, egumus@istanbul.edu.tr*

1. Introduction

The rapid development of network technologies necessitates the performance of systems be high and requirements of the users be provided appropriately. According to traffic pattern, a continuous data transmission or data integrity introduces the expectation of quality of service (QoS). In addition, limited sources like frequency require the source management be planned efficiently. Thus, analysis of system performance and designing of new mechanisms that fulfil system requirements effectively are necessities.

Performance analysis methods are generally simulations, testbeds and predictions for wireless networks. However, when simulations or testbeds are used for analysis, a prior knowledge of all information about the system like the important parameters for network performance: bandwidth, error rate, jitter, throughput or latency, should be present [1]. At this point, usage of machine learning techniques to predict system performance becomes a cost-effective approach. Prediction algorithms need only small amount of information that makes them result faster than other methods. They can be efficiently used to coordinate and optimize network parameters according to changes in traffic where manual adaptation is so difficult due to variety of different type networks [2].
Fast development of data centres increases density of non-real-time data traffic like data backup information transmission and correspondingly causes fluctuations on real-time user's traffic. To prevent this, traffic prediction algorithms can make the non-real-time traffic be transmitted at the time when real-time traffic density is low. In the light of all these advantages, machine learning techniques become more preferred than the other ones for next generation network systems.

In this study, a Generalized Regression Neural Network (GRNN) based prediction model is presented for analysis of DMesh network simulation which is one of the rising next generation network architectures with its numerous advantages [3]. The prediction model estimates *packets dropped* rate in the network simulation using various inputs like *number of gateways*, *number of nodes*, *number of channels used*, and *traffic density*. Predictions of the model are compared to actual outputs of the simulation. Results prove that by using sufficient number of observations, GRNN based prediction model can represent real characteristics of DMesh architecture only with tolerable amount of error. Throughout the study, topics like the relation between traffic density and prediction error, and determining the required number of observations for prediction are also issued.

Rest of the paper is organized as follows: Section 2 presents some of previous studies about prediction techniques used for network performance analysis. Section 3 gives brief information about DMesh architecture, its simulation and GRNN approach. Experimental results are given in Section 4. Finally, the study is concluded in Section 5.

2. Studies on Traffic Analysis

Machine learning techniques became popular for performance evaluation of computer networks because of their significant advantages. There are many studies that benefit from machine learning techniques.

Machine learning techniques are invoked frequently and new methods are proposed since maintenance and operation of network is crucial for Software Defined Networks (SDNs) which have complex network traffic. EMD-based multi-model prediction (EMD-MMP) [2] algorithm that is proposed for short-term traffic forecasting combines traditional prediction methods with the EMD to improve the network prediction accuracy by referring characteristics of EMD for simplifying complicated data.

One of the most important challenges for network analysis is link prediction. It is used to detect illegal and hidden organizations at social security networks while human behaviour is analyzed at social networks. In [4], link prediction problem at probabilistic temporal uncertain networks is handled. Studies using machine learning for link prediction are analyzed and a new method based on random walk algorithm is proposed. This new method combines temporal and global topological information with higher quality than existing studies.

Environmental monitoring is a popular application example of wireless networks. Constraints like battery life cause scaling problems while environmental monitoring with the help of Wireless Sensor Networks (WSN). Three processing steps are followed during environmental monitoring on a WSN: prediction, compression and recovery. A new framework, proposed in [5], compounds these steps. Least mean square (LMS) is used for data prediction at both node and cluster head, then central Principal Component Analysis (PCA) is used for data compression. Finally, base station recovers original data with error tolerance. Combination of these three steps makes this framework cost-effective.

There are various factors affecting performance of a network such as network size, mobility of network, and so on. Therefore, design of routing protocols must be handled carefully. During this design procedure, network behaviour is needed to be analyzed, efficiently. It is possible to associate protocol performance with metrics by using regression models. In [6], an adaptive control method that uses Protocol Regression Model (PRM) to select most suitable routing algorithm for the case network is proposed. By this way, instead of designing a new protocol, it is proved that existing protocols can be used effectively where a unique routing protocol fails for all possible environmental conditions and requirements.

WMNs have infrequency in terms of traffic change since they have a large number of end users. This characteristic of WMN makes traffic classification become complicated. In [7], an online traffic classification tool is developed. Semi-supervised architecture of the tool is its strong suit and makes it

possible to achieve high performance with less data samples.

3.Materials and Methods

This section presents brief information about the Mesh network simulation and regression methodology subject to this study.

3.1. DMesh (Directional Mesh Architecture)

Wireless Mesh Networks (WMNs), a kind of multi-hop ad hoc networks, are in place among next generation networks with their significant benefits such as easy maintenance, high security, self-configuration, low cost and robustness [8, 9]. Features like broadband access and rapid fixing of connection failures make them usable as emergency or disaster communication systems [10].

A typical WMN consists of three layers: gateways, mesh routers and clients. Gateways work as bridges to connect WMN to other networks. Mesh routers that are responsible for receiving/transmitting data packets from/to other networks, have special abilities in addition to basic ones. Mesh clients are combinations of fixed and wireless mesh devices that use WMN services. Mesh clients may compose a client mesh network among themselves or with mesh routers.

In multi-channel multi-radio (MC-MR) WMNs systems, each mesh router can be equipped with multiple antennas to increase network overall capacity. Thus, a router that equipped with various radio interfaces can communicate with multiple routers simultaneously. A well-planned channel assignment (CA) algorithm is responsible for adjustment of each antenna to different channels. By this way, it provides minimization of interference between the channels and ensures setting up proper data paths between the nodes.

DMesh is the first architecture that uses directional antennas with an omnidirectional antenna to the best of our knowledge [3]. Usage of inexpensive and easy-setup feature directional antennas brings on DMesh the best performance among similar architectures. DMesh ensures effective frequency usage by its conservative channel assignment scheme while it increases the inference level of the network.

In this section, dynamic and distributed CA scheme that is used by DMesh architecture and called as C-DCA is proposed. C-DCA is a dynamic and distributed CA method that aims to increase throughput of MC-MR WMNs. DMesh combines spatial separation in directional antennas with frequency separation in orthogonal channels. In this way, more transmissions with less interference are achieved. Besides, DMesh benefits from the advantages of practical directional antennas like inexpensiveness and wide beamforming.

There are several studies to improve throughput of MC-MR WMNs in the literature [11, 12]. However, in these studies, just omnidirectional antennas are used on the routers that increases interference level of the

network. That is, increasing throughput while decreasing interference goal of CA schemes fails. On the other hand, DMesh overcomes this dilemma with its distributed and dynamic CA scheme (C-DCA). DMesh follows three steps on CA procedure: composing a physical tree of which root(s) is/are gateway node(s), routing packets through the network and performing CA scheme.

The routing process is called as Directional Optimized Link State Routing (DOLSR), which is an extended version of Optimized Link State Routing (OLSR) [13] obtaining multi-hop routes in single-radio single-channel omnidirectional mesh networks [3].

3.2. Generalized Regression Neural Networks (GRNNS)

Artificial Neural Networks (ANNs) are layered structures consisting of interconnected nodes called "neurons", inspired by biological neurons. Connection between each node pair is rated with tunable weights which are adjusted by a series of input patterns and their corresponding outputs. This adjustment process is known as "learning" or "memorizing", and achieved by using various learning rules [14]. With their customizable structure, ANNs have the valuable property of generalization for revealing complex relations between inputs (X) and targeted outputs (Y).

ANNs can be employed for a wide range of learning tasks. In this context, Generalized Regression Neural Networks (GRNNs) [15, 16] are their specialized versions for regression. GRNNs are a type of radial basis networks used for function approximation. They are usually composed of two layers: input layer (radial basis layer) and output layer (linear layer). Input layer produces the net input $\Sigma_i = \| X_p - W_i \| b(i)$ of ith neuron, where $b(i)$ is the bias term, and $\| X_p - W_i \|$ is the Euclidean distance between the input pattern X_p and weight vector W_i of ith neuron. The net input is fed to radial basis function $f(x) = e^{-x^2}$, normalizing each output of first layer to 0-1 range. The output is obtained by application of linear transfer function $g(x) = x$ on net input of the output layer. A typical GRNN is shown in Fig. 1. Here, X_p and Y_p correspond to pth input/output patterns.

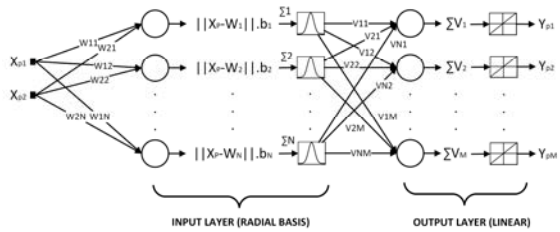

Fig.1 General form of generalized regression neural network.

3.3. DMesh Simulation

DMesh simulation was prepared using Matlab [17]. Specifications of the simulation are presented in Table 1.

The network simulation is driven by four parameters: *number of gateways*, *number of nodes*, *number of channels used*, and *traffic density* affecting the outcome *packets dropped rate* (%).

Number of gateways, *number of nodes*, and *number of channels used* are predetermined at the beginning of the simulation. Besides, the location information (coordinates) and deviation angles of each node are set randomly. After forming the network logically, routing trees are set up and CA is handled.

Table 1. Specifications of DMesh simulation

Simulation area	500m × 500m
Number of gateways	Varies between 1-10 (incremented by 1)
Number of nodes	Varies between 10-200 (incremented by 10)
Number of usable channels	3, 6 or 12
Deviation angle of a directional antenna	Chosen randomly between $[\ 0, \frac{\pi}{2}\ ]$
Traffic Density	Varies between 10%-100% (incremented by 10%)
Traffic model	Poisson
Packet Size	1500 bytes
Bit rate	54 Mbps
Simulation time	100 sec

A typical network architecture formed using the simulation is illustrated in Fig. 2.

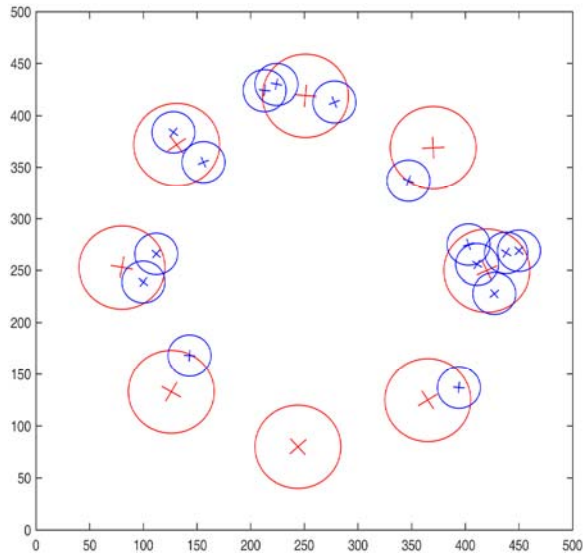

Fig. 2. A 12-channel Mesh topology with 8 gateways (red circles) and 15 nodes (blue circles).

4. Results

In order to evaluate the performance of GRNN predicting the drop rate, three distinct regression networks were created with *number of gateways* and *number of nodes* as the inputs and *packets dropped* rate as the output. Each one of the three networks corresponded to a simulation with specific number of channels (3, 6, or 12) used. The data set contained 6000 observations which were split into ten distinct groups according to *traffic density* parameter and half of the samples from each group were fed into corresponding network for training. After training process, remaining half of the samples were fed into the network and predictions were obtained. In order to eliminate the bias effect, this train-test process was repeated 100 times for each group using random permutations of samples for training/testing. Mean values of outputs

(*packets dropped rate*) for each test sample were calculated and stored as predictions of corresponding GRNN. Fig. 3 depicts observations and predictions of the three GRNNs with the *traffic density* parameter of 50%.

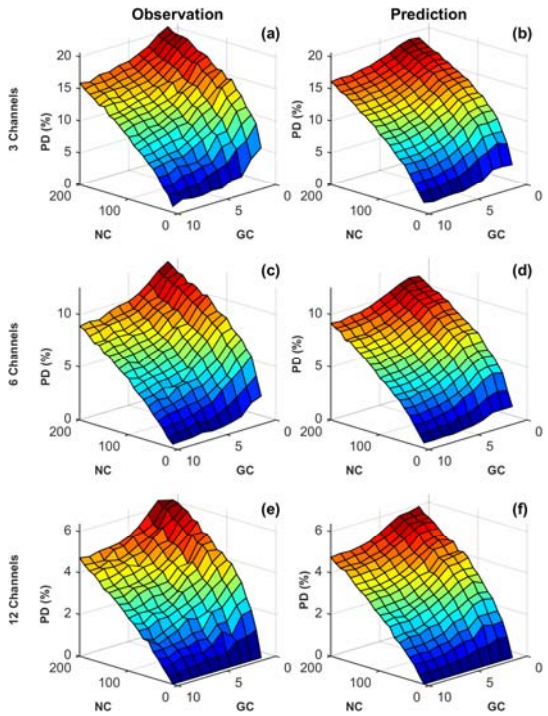

Fig. 3 Observations and corresponding predictions for various channels (NC: Node count, GC: Gateway count, PD: Packets dropped).

As can be seen from Fig. 3(a)(c)(e), *packets dropped* rate falls as the *number of channels used* rises. This is directly a result of reduced number of collisions. Besides, it can also be stated that *number of nodes* (NC) and *number of gateways* (GC) parameters have opposite effects on *packets dropped*. Coming to our main concern, Fig. 3(b)(d)(f) verify that predictions of GRNNs present same characteristics as observations which can be seen from explained variance values given in Table 2. High values are indicators of goodness of fit. The characteristics seem not to depend on *traffic density*.

Table 2. Explained variance of trained GRNNs.

Traffic Density	Variance Explained		
	3 Channels	6 Channels	12 Channels
10%	0.9611	0.9628	0.9697
20%	0.9604	0.9641	0.9691
30%	0.9617	0.9641	0.9692
40%	0.9612	0.9632	0.9692
50%	0.9614	0.9623	0.9685
60%	0.9613	0.9626	0.9687
70%	0.9616	0.9627	0.9680
80%	0.9605	0.9643	0.9682
90%	0.9607	0.9627	0.9693
100%	0.9608	0.9636	0.9688

Although having same characteristics, predictions are not identical to observations which are the main concept of "generalization". Fig. 4 presents the variation in prediction error (Root Mean Squared Error) according to the change in *traffic density*. The *packets dropped* rate rises as the *traffic density* rises, yielding to more diverse observations and an increment in RMSE. On the other hand, the reduction in *number of channels used* increases *packets dropped* rate which explains higher RMSE values obtained from GRNNs of smaller *number of channels.*

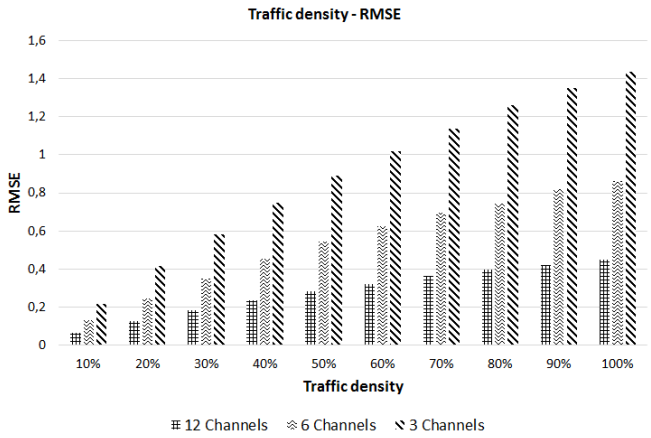

Fig. 4. Variation in RMSE according to traffic density.

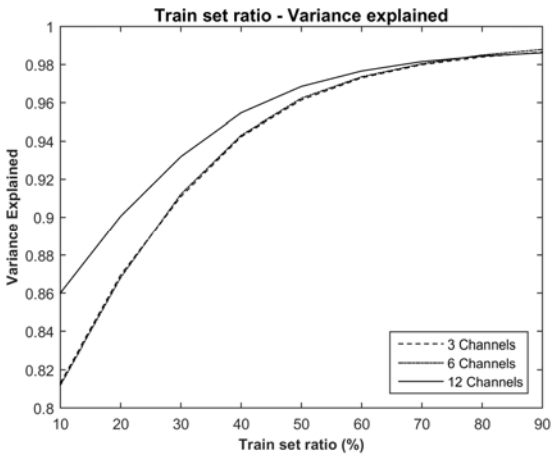

Fig. 5. Train set ratio - Variance explained.

As stated before, presented results were obtained by using 50% of samples for training and the remaining 50% for testing, in several trials. This choice of split provided a high explained variance value of 0.96 (see Table 2) for all of the three GRNNs meaning that predicting the *packets dropped* rates of *N* cases could be achieved by using *N* observations. As might be expected, changing the ratio of train set size can affect the generalization performance. Fig. 5 presents the change in variance explained according to increasing ratio of training set size. It can be clearly seen that the GRNNs that were trained by samples of 3 and 6 channels exhibit same manner and their explained variance values overlap. However, the GRNN for 12 channels presented a better generalization performance. All of the three networks meet at explained variance value of 0.98, when using 70% of samples for training, which seems to be a peak. Some might also choose this as preferred train split ratio.

5. Conclusions

Determination of the factors that affect the performance of a network system is substantial in the way of facilitating to make proper regulations. A method for evaluation of network performance needs to be successful in addition to providing an efficient approach in terms of speed and cost. In this context, using machine learning methods offers faster and cost-effective results using only small amount of data in order to predict system behaviour. This provides these methods be mentioned along with other methods for network performance analysis.

In this study, generalized regression neural networks (GRNNs) approach was employed in order to predict the output, *packets dropped,* of test cases. Although, four inputs determine the output, only *number of gateways* and *number of nodes* were used as inputs of separate networks in order to evaluate effect of *number of channels used* and *traffic density* on regression. The *traffic*

density parameter did not seem to influence the explained variance, however, it had a direct impose on RMSE due to its effect on output. On the other hand, *number of channels used* parameter also had a direct impose on RMSE, but due to its inverse proportion to the output, this impose was also in opposite way.

In addition to these, effect of train/test split was also examined. Results proved that, by choosing an ideal proportion for training, GRNNs can provide high explained variance and low RMSE values which are indicators of goodness of fit. This makes them good candidates for estimating output parameters of DMesh architecture.

Acknowledgements
Authors thank Assoc. Prof. Dr. Olcay Kursun from the same department for helpful discussions.

REFERENCES

[1] Rappaport T.S., *Wireless communications: principles and practice (2nd edition)*. Upper Saddle River, NJ: Prentice Hall PTR. ISBN 0-13-042232-0, 2002.

[2] Dai L., Yang W., Gao S., Xia Y., Zhu M., and Ji Z., "EMD-based multi-model prediction for network traffic in software-defined networks," *in IEEE 11th International Conference on Mobile Ad Hoc and Sensor Systems (MASS)*, Philadelphia, PA, pp. 539-544, 2014.

[3] Das S.M., Pucha H., Koutsonikolas D., Hu C., and Peroulis D., "Dmesh: Incorporating practical directional, antennas in multi-channel wireless mesh networks," *in IEEE J. Sel. Areas Commun.*, vol. 24, no. 11, pp. 2028-2039, 2006.

[4] Ahmed N.M., and Chen L., "An efficient algorithm for link prediction in temporal uncertain social networks," *Information Sciences,* vol. 331, pp. 120-136, 2016.

[5] Wu M., Tan L., and Xiong N., "Data prediction, compression, and recovery in clustered wireless sensor networks for environmental monitoring applications," *Information Sciences,* vol. 329, pp. 800-818, 2016.

[6] Priya S.B.M., "Adaptive control of routing protocol in mobile adhoc network using regression model," *in International Conference on Emerging Trends in Science, Engineering and Technology (INCOSET)*, Tiruchirappalli, Tamilnadu, India, vol. 13-14, pp. 509-514, 2012.

[7] Gu C., Zhang S., Xue X., and Huang H., "Online wireless mesh network traffic classification using machine learning," *Journal of Computational Information Systems,* vol. 7, no. 5, pp. 1524-1532, 2011.

[8] Alzubir A., Bakar K.A., Yousif A., and Abuobieda A., "State of the art, channel assignment multi-radio multi-channel in wireless mesh network," *International Journal of Computer Applications,* vol. 37, no. 4, pp. 14-20, 2012.

[9] Riggio R., Pellegrini F.D., Miorandi D., and Chlamtac I., "A knowledge plane for wireless mesh networks," *Ad Hoc & Sensor Wireless Networks,* vol. 5, pp. 293-311, 2007.

[10] Yarali A., Ahsant B.., and Rahman S., "Wireless mesh networking: a key solution for emergency&rural applications," *in IEEE Second International Conference on Advances in Mesh Networks*, pp. 143-149, 2009.

[11] Draves R., Padhye J., and Zill B., "Comparison of routing metrics for static multi-hop wireless networks," *in Conference on Applications, technologies, architectures, and protocols for computer communications (SIGCOMM),* pp. 133-144, 2004.

[12] Raniwala A., and Chiueh T., "Architecture and algorithms for an IEEE 802.11-based multi-channel wireless mesh network," *in 24th Annual Joint Conference of the IEEE Computer and Communications Societies*, New York, pp. 2223-2234, 2005.

[13] Received from: https://tools.ietf.org/html/rfc3626

[14] Zurada J.M., *Introduction to artificial neural systems.* West Publishing Co., St. Paul, MN, USA, 1992.

[15] Specht D.F., "A general regression neural network," *IEEE Transactions on Neural Networks*, vol. 2, no. 6, pp. 568-576, 1991.

[16] Wasserman P.D., *Advanced methods in neural computing.* New York, Van Nostrand Reinhold, pp. 155-61, 1993.

[17] MATLAB Release 2015a, The MathWorks, Inc., Natick, Massachusetts, United States.

An Optimization Model and Genetic Algorithm Solution for Software Projects

***Yucel DIL*[1]**
***Mustafa Cem KASAPBASI*[2]**

Abstract
Many optimization techniques which are inspired by the nature are used in optimization problems. Genetic Algorithms (GA) is an optimization algorithm, tries to mimic the natural process of livings. Allowing to survive better generation therefore inheriting the better qualifications to next generations. In this study genetic algorithm is used to find the optimal cost for a software project. In order to evaluate results of the genetic algorithm, a test system based on linear programming is established. The results indicates that designed genetic algorithm optimization model successfully calculated the cost of software project very close to deterministic costs.

Keywords: *Software project management, genetic algorithm, optimization.*

1. Introduction

Software project management aims to achieve all the project goals and objectives while working within the constraints posed by project environment and stakeholders. These constraints include (but not limited to) time, scope, resources, resource allocation and optimization etc. [1].

Software project management (SPM) is the art and science of planning and leading software projects [2]. According to [4] a survey conducted in the industry only about a quarter of software projects are regarded as successful therefore billions of dollars are lost annually due to the project failures or unsatisfactory project deliveries. Many problems can cause such results but it is mainly because of failing to understand and manage software project risks [5], also not having a proper quantitative cost calculation tool therefore letting the project being guided by subjective decisions of project manager. Unable to comprehend project entirely may lead problems like cost schedule overruns, unmet user requirements.

Software management can be defined as keeping team together on the same purpose, distributing tasks while keeping healthy intercommunication between team members,

[1] *Computer Engineering Department, Istanbul Commerce University, Istanbul, Turkey, yuceldil@gmail.com*
[2] *Computer Engineering Department, Istanbul Commerce University, Istanbul, Turkey, mckasapbasi@ticaret.edu.tr*

at the end of each task evaluating results properly to asses overall progress [6].

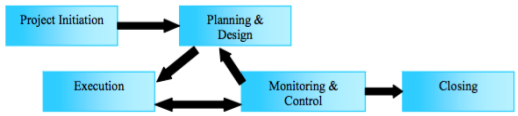

Fig. 1. Traditional Project Management Stages [1]

2. Background Study and Methodology

Literature Review

Since Software Project Management is considered a subclass of Project Management there are many researches, tools and methodology could be used to assess software projects. However software project managements are highly depended on manager's subjective judgments. Therefore some means of quantitative tools and decision helpers are needed for various stages of Software Projects.

One of such stage is Risk Control of a software project management. In [3] Capability Maturity Model based (CMM) risk assessment system is proposed. In that study previous similar project results are used as database in obtaining the problem solution via a dynamic programming method. Another Risk Control optimization model is proposed in [5] utilizing particle swarm optimization methodology to represent some means of quantitative data to software project manager.

Another approach is to determine the software metrics and modeling them to assist the software project manager. A successful fuzzy model for software metrics is presented to better analyze the time vs. performance vs. information vs. cost tradeoffs that are entailed in software project management [7].

3. Methodology and Application

Same software project management experiment scenario is conducted for two different methods namely Linear Programming and Genetic Algorithm, which are used to optimize the cost of the project. At the end, these two methods are compared weather they are consistent with each other.

Conducted Experiment Scenario

In the software project 10 people are going to be allocated 6 of them are process analysts, 4 of them are software

Table 1. Man Hours Distribution and Cost of the Workers, Variable Names of Cost Function

Worker	Work (man hour)												Wages per Hours (TL)
	Analysis			*Coding*			*Testing*			*Activating*			
	Cost	*LP Cost*	*Variable name*	*Cost*	*LP Cost*	*Variable name*	*Cost*	*LP Cost*	*Variable name*	*Cost*	*LP Cost*	*Variable name*	
D_1	-	-	-	84	3192	X_1	78	2964	X_2	66	2508	X_3	38
D_2	-	-	-	82	2296	X_4	80	2240	X_5	64	1792	X_6	28
D_3	-	-	-	102	2448	X_7	78	1872	X_8	68	1632	X_9	24
D_4	-	-	-	106	2756	X_{10}	76	1976	X_{11}	68	1768	X_{12}	26

A_1	70	1960	X_{13}	-	-	-	66	1848	X_{14}	54	1512	X_{15}	28
A_2	94	2256	X_{16}	-	-	-	52	1248	X_{17}	56	1344	X_{18}	24
A_3	78	2964	X_{19}	-	-	-	58	2204	X_{20}	62	2356	X_{21}	38
A_4	86	3096	X_{22}	-	-	-	70	2520	X_{23}	60	2160	X_{24}	36
A_5	112	2240	X_{25}	-	-	-	64	1280	X_{26}	52	1040	X_{27}	20
A_6	102	2244	X_{28}	-	-	-	72	1584	X_{29}	50	1100	X_{30}	22

developers. Qualifications and experience of these people also the cost of them are known from previous projects in which they have involved.

This software project consists of 4 main phases namely analyzing (Planning & Designing), writing codes (Execution), testing (Monitoring & Control), and activating the project (Closing). These phases comply with the generic project management process that can be seen from Fig. 1. In Table 1 according to job assignments of workers, unit costs are given Turkish Lira and man hours are depicted accordingly. D stands for Developer, A stands for Analyst. As can be inferred from the Table 1 that some analysts and developers cost more then others since they have different experience levels.

As in every project this project has constrains that are guaranteed by the contract signed by parties. Complying these constraints is one of the responsibilities of the software project manager.

- It is expected that every developer must work at least 8 hours and every analyst must spent at least 16 hours on the project.
- Maximum 86 hours for coding, 100 hours for analysis, 80 hours for tests, and for activating project 64 hours must be separated.
- According to accepted quality assurance standard of the company at least 82 hours for coding, 80 hours for analyzing, 56 hours for testing and 60 hours for activating the project must be separated.

It is expected from and responsibility of the software project manager that while being coherent with the constraints obtaining the minimum cost with the optimum resource planning.

Project is regarded and designed as a minimization focused optimization problem. This problem is solved using with Linear Programming (LP) and Genetic Algorithms (GA) then results are compared with each other. For linear Programming Eq.1 is utilized as cost function and minimum cost is obtained accordingly.

$$\begin{aligned} \text{Min } C = {} & 3192\,X_1 + 2964\,X_2 + 2508\,X_3 + \\ & 2296\,X_4 + 2240\,X_5 + 1792\,X_6 + 2448\,X_7 + \\ & 1872\,X_8 + 1632\,X_9 + 2756\,X_{10} + 1976\,X_{11} + \\ & 1768\,X_{12} + 1960\,X_{13} + 1848\,X_{14} + 1512\,X_{15} + \\ & 2256\,X_{16} + 1248\,X_{17} + 1344\,X_{18} + 2964\,X_{19} + \\ & 2204\,X_{20} + 2356\,X_{21} + 3096\,X_{22} + 2520\,X_{23} + \\ & 2160\,X_{24} + 2240\,X_{25} + 1280\,X_{26} + 1040\,X_{27} + \\ & 2244\,X_{28} + 1584\,X_{29} + 1100\,X_{30} \end{aligned} \quad (1)$$

When we have presented this project as mathematically we presented 30 variables and 18 constraints. MATLAB program is utilized to solve the same problem with Genetic Algorithm.

Table 2. Results of Both LP and GA Optimization

Workers and Stage Steps	Working Time Constraints	Lineear Programming		Genetic Algorithm	
		Work Duration	Deviation (%)	Work Duration	Deviation (%)
D1	$X_1 + X_2 + X_3 >= 8$	8	0	8	0
D2	$X_4 + X_5 + X_6 >= 8$	58	0,5	68,2	0,6
D3	$X_7 + X_8 + X_9 >= 8$	8	0	8	0
D4	$X_{10} + X_{11} + X_{12} >= 8$	8	0	8	0
A1	$X_{13} + X_{14} + X_{15} >= 16$	80	0,64	77,64	0,62
A2	$X_{16} + X_{17} + X_{18} >= 16$	40	0,24	43,98	0,28
A3	$X_{19} + X_{20} + X_{21} >= 16$	16	0	16	0
A4	$X_{22} + X_{23} + X_{24} >= 16$	16	0	16	0
A5	$X_{25} + X_{26} + X_{27} >= 16$	28	0,12	16	0
A6	$X_{28} + X_{29} + X_{30} >= 16$	16	0	16,17	0
Coding	$82 <= X_1 + X_4 + X_7 + X_{10} <= 86$	82	0	82	0

Analysis	$80 <= X_{13} + X_{16} + X_{19} + X_{22} + X_{25} + X_{28} <= 100$	80	0	80	0
Test	$56 <= X_2 + X_5 + X_8 + X_{11} + X_{14} + X_{17} + X_{20} + X_{23} + X_{26} + X_{29} <= 80$	56	0	56	0
Activating	$60 <= X_3 + X_6 + X_9 + X_{12} + X_{15} + X_{18} + X_{21} + X_{24} + X_{27} + X_{30} <= 64$	60	0	60	0
Project Cost		523.600 TL		533.919 TL	
Total Deviation		1,46		1,5	
Solution Time		0,301884 sn		2,029242 sn	

After 200 generation desired solution has obtained for GA. While calculating with GA Linear generation function is preferred for generating generations. Two point crossover method is chosen for crossover function. For selection process Tournament method is preferred. Same constraints and fitness function is used for evaluation as use in LP. Results are depicted in Table II. As one can understand from the Table II that cost calculation of LP and GA are both similar.

After Project Non Linear Programming

After the project minimum cost is applied and being used. Due to quality control standards requirements each cost of application used in the project can be calculated in a certain tolerance of error. If this rate of error goes beyond the pre determined tolerance new version of cost calculation is carried out.

Error rate that will be experienced according to usage amount (number of steps) is chosen as $2X_1^{0,1}$. This error rate corresponds and composed of due to misusage and application.

In Eq. 2 X_1 represents number of steps, X_2 represents number of errors due to misusage. Relation of number of steps and error due to misusage is depicted in Eq. 2.

$$F(X) = X_1^{0,3} + 2X_2^{0,2} \quad (2)$$

It is desired from project manager to assign and work with maximum number of users in the project without publishing e new version of the cost calculation and schedules. Since these calculations always alter the initial plan therefore modifies it.

The constraints that should be take in to consideration by the project manager are as fallows:

In the case errors due to application rises over 75 a new application release should be calculated and presented. This constraint is illustrated in Eq. 3.

$$2X_1^{0,1} - X_2 <= 75 \quad (3)$$

Total number of errors must be less then 100. This constraint is illustrated in Eq. 4.

$$2X_1^{0,1} <= 100 \quad (4)$$

All of the errors can not be resulted from misusage. This constraint is illustrated in Eq. 5 and Eq. 6.

$$2X_1^{0,1} - X_2 >= 0 \quad (5)$$
$$X_1 >= 0, X_2 >= 0 \quad (6)$$

Even in this case what is expected from the project manager is also considered and investigated as an optimization problem. Designed problem is non linear and have non linear constraints Cases of which are regarded as hard solution problems. In order to solve the problem MATLAB program is utilized.

4. Conclusions

In this study cost optimization problem of software project is analyzed using GA applied to LP and Non LP. Sample constraints and cases that can be encountered in a software project are chosen. As a result it has been emphasized that software development projects can be designed as an optimization problem and a solution can be proposed to the problems may be encountered while activating the project. Another contribution is the use of Genetic Algorithm approach in software project management processes.

REFERENCES

[1] Ramzan, M.; Iqbal, M.A.; Jaffar, M.A.; Rauf, A.; Anwar, S.; Shahid, A.A., "Project Scheduling Conflict Identification and Resolution Using Genetic Algorithms," in *Information Science and Applications (ICISA), 2010 International Conference on* , vol., no., pp.1-6, 21-23 April 2010 doi: 10.1109/ICISA.2010.5480400

[2] Stellman, Andrew; Greene, Jennifer. "Applied Software Project Management". O'Reilly Media, 2005

[3] Xu Ruzhi; Qian leqiu; Jing Xinhai, "CMM-based software risk control optimization," in Information Reuse and Integration, 2003. IRI 2003. IEEE International Conference on , vol., no.,

pp.499-503, 27-29 Oct. 2003 doi: 10.1109/IRI.2003.1251457

[4] Kwak, Y. H., & Stoddard, J. (2004). Project risk management: Lessons learned from software development environment. Technovation, 24(11), 915–920.

[5] Ping Cao; FuJi Chen, "A Risk Control Optimization Model for Software Project," in Computational Intelligence and Software Engineering, 2009. CiSE 2009. International Conference on , vol., no., pp.1-4, 11-13 Dec. 2009 doi: 10.1109/CISE.2009.5362886

[6] Güney D. D.,Yönetim ve Organizasyon. Nobel Publishing Dağıtım 2007.

[7] Mirseidova, S.; Atymtayeva, L., "Definition of software metrics for software project development by using fuzzy sets and logic,", Joint 6th International Conference on Soft Computing and Intelligent Systems (SCIS) and 13th International Symposium on Advanced Intelligent Systems (ISIS), 2012 vol., no., pp.272-276, 20-24 Nov. 2012doi: 10.1109/SCIS-ISIS.2012.6505336

Control of Fuel Cell Power System

Ayse KOCALMIS BILHAN[1]
Caisheng WANG[2]

Abstract
In recent years, it is getting attention for renewable energy sources such as Fuel Cell (FC), batteries, ultracapacitors or photovoltaic panels (PV) for distributed power generation systems (DG) or electrical vehicles. This paper proposes a DC/DC converter and DC/AC inverter scheme to combine the Fuel Cell Stack (FC). The power system consist of a FC stack, a DC/DC converter, inverter and load. A FC mostly could not produce necessary output voltage, the DC/DC boost converter is used for obtaining the desired output voltage. The inverter is used for many applications such as electrical vehicles (EV) and distributed generation systems (DG). In this paper, sinusoidal pulse modulation technique and space vector pulse width modulation technique have been simulated and compared for electrical vehicles applications.

Keywords: *Converters, Fuel Cells, Electrical Vehicles*

1. Introduction

Increasing human population brings some requirements such as clean water, clean air and much more electrical energy [1]. Also many research results show that fossil-based energy sources have become running out and also fossil-based energy sources cause to environmental pollution (air, ozone hole and etc.). In the last decade, more attentions have been given to renewable energy technologies such as solar, wind, geothermal, biomass, hydraulic and FCs. Advantages of all these kind of energy sources are that they do not run out and do not cause environmental damages due to the usage of fossil energy sources such as coal, natural gas and etc. In the near future, they will be the answer for addressing pollution, global warming, potential energy crisis, and etc. Recently all renewable energy technologies are very popular and widely used around the world.

FCs can be used as a primary energy source for distributed power generation (DG) [2], electrical vehicles (EV), residential application or transportation because of they can be fabricated without environmental pollution or efficiency. It can be considered as a voltage sources or a power plant or a battery. FCs are electrochemical energy converter which convert chemical energy of a fuel directly into an electrical energy. It is very clean energy source because of water is only by-product. The output power generating

[1] *Nevsehir H.B.V. University, Nevsehir, Turkey, akbilhan@nevsehir.edu.tr*
[2] *Wayne State University, MI, USA*

capacity can be easily increased by adding more FC modules. Advantages of FCs can be listed as [3];

- High efficiency,
- High reliability,
- Not-moving part, and modular
- Do not cause pollution.

The main source of FC is hydrogen. The hydrogen (H_2) is the most abundant element but unfortunately it does not appear naturally in a useful form. Almost half of hydrogen is produced by steam reforming of natural gas. The other methods of producing hydrogen are electrolysis of water, conversion of coal to H_2, use of biomass energy to produce H_2, use of nuclear energy (NE) to produce H_2 or use of solar energy to produce H_2.

This paper describes design of suitable control strategies for FC DG systems to keep system stable with RL load. A Matlab/Simulink model is built in the proposed work.

A FC has an electrolyte layer between an anode and a cathode electrodes. In the literature many FCs structures have been developed and they are classified according to types of electrodes and electrolytes used inside [4]: Proton Exchange Membrane FC (PEMFC), Solid Oxide FC (SOFC), Molten Carbonate FC (MCFC), Phosphoric Acid FC (PAFC), Alkaline FC (AFC) and etc. [5]. A schematic representation of a FC is shown in Fig. 1.

PEMFCs are commonly known as proton exchange membrane fuel cells which are used a solid polymer as electrolyte. This electrolyte is an excellent conductor of protons and an insulator of electrons the overall reaction of PEMFC can be summarized with Eq. (1), (2) and (3). These reactions proceed continuously.

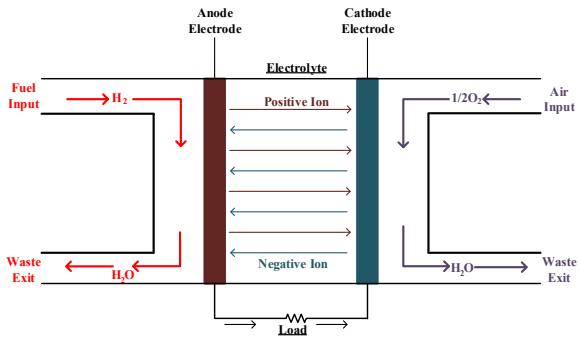

Fig.1 A schematic representation of a FC

Anode Reaction: $H2 \rightarrow 2H^+ + 2e^-$ (1)

Cathode Reac.: $\frac{1}{2} O_2 + 2H + 2e^- \rightarrow H_2O + Heat$ (2)

Overall Reaction: $H_2 + 1/2\ O_2 \rightarrow H_2O + Heat$ (3)

PEMFCs have been used in worldwide in many type applications such as hospitals, shelters, offices, hotels and schools [6]. PEMFCs can be used either main power sources or back up units. Each cell in a FC stack has a low output voltage (around 1V at full load), it is necessary to stack many in series to obtain a reasonable output voltage. For low power applications the number of cells that needs to be connected in series is small, but as power increases the number of cells that are required in the stack increases rapidly and it is called as a FC Power Plant (FCPP). In Fig. 2, a basic diagram of a FCPP has been shown. Also numbers of usage FC can be calculated by using Eq. (4) and Eq. (5)

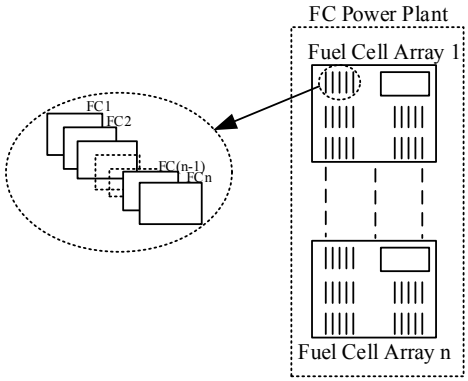

Fig.2 The basic diagram of FCPP

$$N_s = \frac{\text{FC System Voltage}}{\text{FC Stack Voltage}} \quad (4)$$

$$N_p = \frac{\text{FC System Power}}{\text{FC Stack Power}} \quad (5)$$

The main purpose of using FCs is to produce stable DC output voltage independent of the load current. Unfortunately, the FC mostly could not produce necessary output voltage. Also a FC has not storage capability, response slowly and the output voltage has ripples with loads. For these reasons in many applications show that a FC stack needs a supporting system [6] such as DC/DC converter, ultracapacitors (UC), high voltage battery and/or energy management systems.

2. The Fuel Cell Power System

In Fig. 3, Block diagram of whole system has been shown. "Fuel Processing Unit" and "Fuel Cell" blocks produce DC voltage by using fuel and air. In the "Power Convertion Unit" block, the output voltage of FC is increased by using DC/DC boost converter and converted to AC output voltage by using DC/AC converter. Finally, "Control Unit" block control switching signals of DC/DC and DC/AC converters.

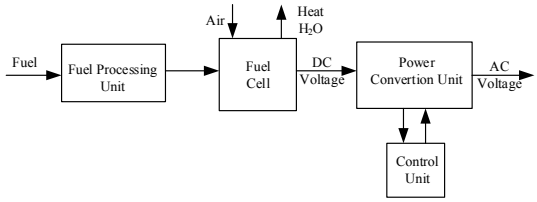

Fig.3 Block diagram of whole system

2.1. Fuel Cell

A FC equivalent circuits are shown in Fig. 4 [7]. V_{ccell} (concentration), $V_{actcell}$ (activation), $V_{ohmcell}$ (ohmic) show voltage drops in FC in Fig. 4(a). These voltage drops are functions of load current and FC temperature or pressure. E_{cell} and V_{cell} are reversible voltage and output voltage of FC, respectively.

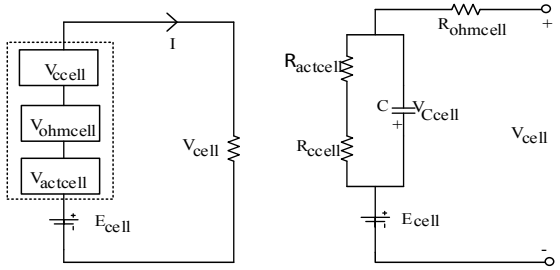

(a) (b)

Fig. 4 FC (a) equivalent circuit, (b) equivalent electric circuit

$R_{ohmcell}$ (ohmic resistance) is a function of FC temperature. R_{ccell} and $R_{actcell}$ are resistances of concentration ad activation voltage components, respectively. The output voltage of a single cell can be calculated by using Eq. (6) [8]. In this paper, the output voltage of the FC is 38,1V.

$$V_{cell} = E_{cell} - V_{actcell} - V_{ohmcell} - V_{ccell} \quad (6)$$

In Eq. (6), E_{cell} is called as Nernst's voltage and it is calculated as Eq. (7);

$$E_{cell}=1.229-0.85x10^{-3}(T-T_{ref})+4.31x10^{-5}T(\ln(P_{H2})+0.5\ln(P_{O2})) \quad (7)$$

where T_{ref} represents the reference temperature, the P_{H2} represents the hydrogen, P_{O2} the oxygen partial pressure, and T represents the cell temperature in K.

2.2. DC/DC Boost Converter

It is necessary to control the output voltage of FC to connect grid. The DC/DC converter boost the voltage, control the FC power and regulate the voltage in the FC applications. In Fig.5, DC/DC boost converter model has been shown.

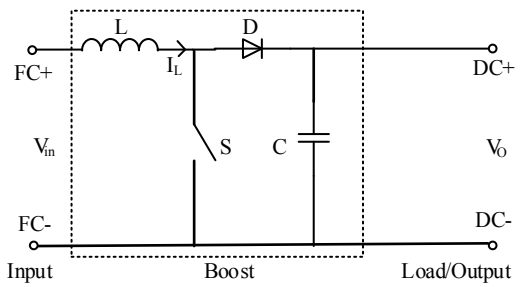

Fig.5 Model of DC/DC Boost Converter

In the boost converter, Eq. (7) and Eq. (8) show if the switch (S) is on and Eq. (9) shows if the switch (S) is off;

$$V_i=\frac{Ldi_L}{dt} \quad (7)$$

$$V_c = V_o \quad (8)$$

$$V_i=\frac{Ldi_L}{dt}+V_o \quad (9)$$

By using Eq. (7), (8) and (9), duty cycle (d) of DC/DC boost converter can be calculated as in Eq. (10).

$$V_i=\frac{V_o}{d-1} \quad (10)$$

In this paper, the boost converter has following parameters; L=3mH and C=200μF. The nominal duty cycle (d) of the boost converter is 2/3. The feedback control of the system has shown in Fig. 6. In this controller K_p is 0.002 and K_i is 0.2.

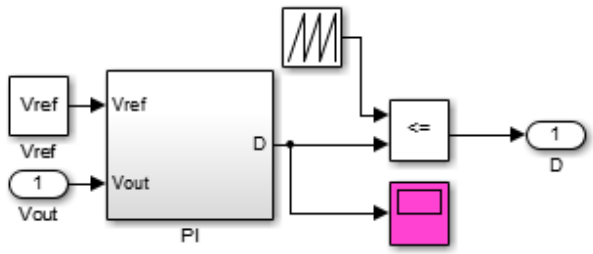

Fig.6 PI Control Structure

2.3. DC/AC Inverter

The inverter convert dc power into ac power with desired magnitude and frequency [9]. It provides flexibility usage of FC in real applications. In Fig.7, the dynamic model of voltage source inverter (VSI) has been shown. The three Phase DC/AC inverter circuit consist of 6 active switches. In the each phase, two IGBT switches are used. The switching frequency is 1,5k Hz.

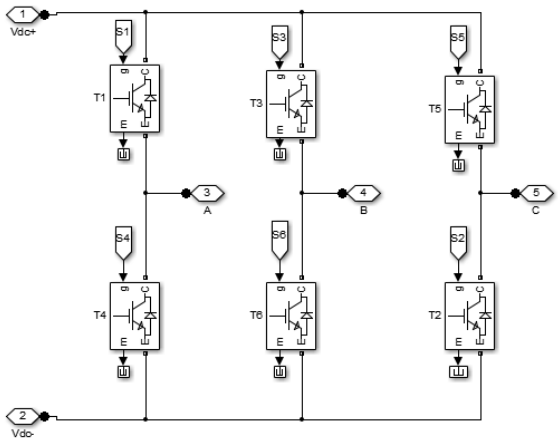

Fig.7 Three Phase DC/AC VSI Inverter

In the literature, several control techniques have been developed such as sinusoidal pulse width modulation (PWM), space vector PWM, sigma-delta PWM and etc [10] for producing output voltage. In the simulation, the output frequency is used as 50Hz, and modulation index of the inverter is used as 0.8.

3. Modelling and Simulation

The performance of the proposed system is simulated by using Matlab/Simulink package program as seen in Fig. 8.

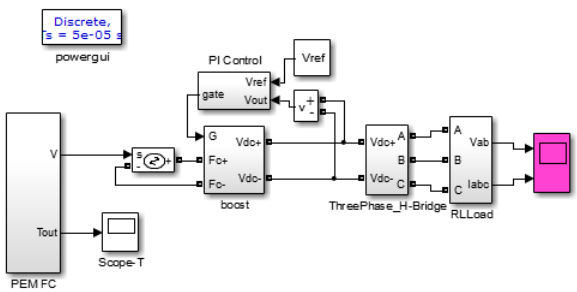

Fig.8 Matlab/Simulink model of whole system

As it seen from Fig. 8, the output voltage of FC cannot be used directly; therefore a step up converter as a boost converter is used. The H-bridge inverter structure is used to convert DC voltage to AC voltage. Finally, a three phase RL load is feed by an inverter structure. In the simulation, R=100Ω and L=0.1H are used as a passive load.

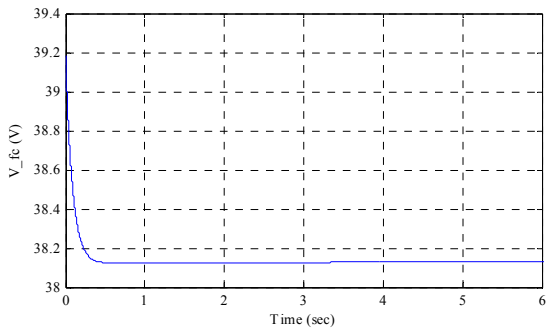

Fig. 9 The output voltage of FC

The output voltage of FC has been shown in Fig. 9 [11] and the output voltage of DC/DC boost converter has been shown in Fig. 10. The duty cycle (d) of the converter is chosen as a 2/3, so the output voltage of the converter is 114,3V.

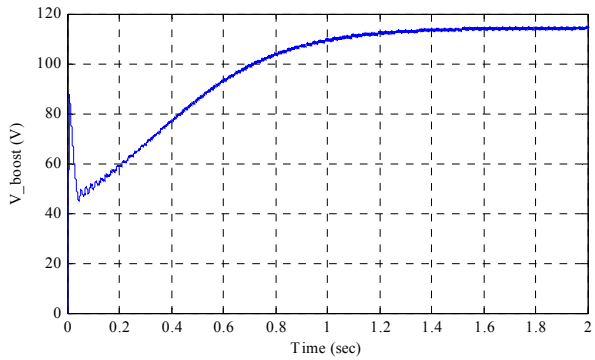

Fig. 10 The output voltage of DC/DC boost converter

The single phase output line current, three phase output current and the line voltage waveforms have been shown in Fig. 11, Fig. 12 and Fig. 13, respectively.

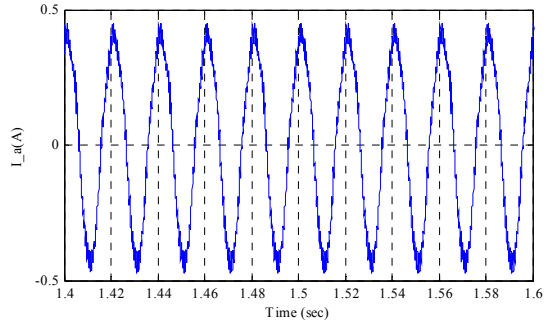

Fig. 11 The single phase output current waveform,
I_a (A)

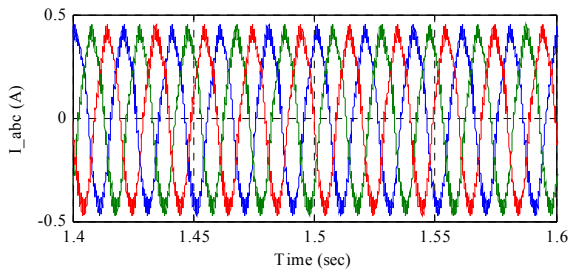

Fig. 12 Three phase output current waveforms,
I_a, I_b,I_c (A)

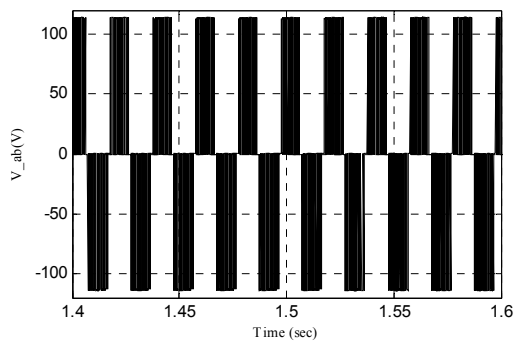

Fig. 13 The three phase output voltage waveform,
V_{ab} (V)

4. Conclusions

A FC power system should be used as a main power source in the near future for DG, EV or portable applications due to it is difficult to find H_2 in useful form and expensive cell components.

In this paper, a FC power system with DC/DC converter and DC/AC inverter is described. The output voltage of FC is considered constant value as 38,1V and the feedback control of DC/DC boost converter has been designed and simulated for the FC power system. By using three phase inverter, it is easy to control output voltage and current.

Recent researches show that improvements of the FCs control algorithms will be getting attention. Also the output voltage control of DC/DC boost converter will be considered in the future works.

Acknowledgement

This work was supported in part by the Scientific and Technological Research Council of Turkey (TUBITAK).

REFERENCES

[1] K. W. E. Cheng, D. Sutanto, Y. L. Ho, and K. K. Law, "Exploring the power conditioning system for fuel cell," *in Proc. IEEE PESC*, 2001,pp. 2197–2202.

[2] Wang, C., Nehrir, M., H., Gao, H., "Control of PEM Fuel Cell Distributed Generation Sytems", *IEEE Trans. on Energy Conversion*, Vol. 21, No.2, pp. 586-595, 2006.

[3] K. Jin, X. Ruan, M. Yang, M. Xu, "A Hybrid Fuel Cell Power System", *IEEE Trans. on Industrial Electronics,* Vol. 56, No.4, pp: 1212-1222, 2009.

[4] Kumar, T. P., Subrahmanyam, N., Syduu, M., "Control Strategies of a Fuzzy Controlled Solid Oxide Fuel Cell/Battery Distributed Generation System for Power Quality Enhancement", *International Conf. on Circuit, Power and Comuputing Tech. (ICCPCT)*, pp. 64-69, 2014.

[5] Chaudhary, S., Chauhan, Y.K., "Studies and Performance Investigations on Fuel Cells", *IEEE International Conference on Advances in Engineering & Technology Research (ICAETR - 2014),* August 01-02, 2014, India.

[6] Barbir F., "PEM Fuel Cells: Theory and Practice", Elsevier, *Academic Press Sustainable World Series*, 2005.

[7] Nehrir, M. H., Wang, C., "Modeling and Control of Fuel Cells", Wiley, *IEEE Pres.,* 2009.

[8] Milanovic, M., Rodic, M., Truntic, M., "DC-DC Conditioning System for FC application", *EPE/PEMC Conference*, pp: DS3d.3-1-DS3d.3-5, 4-6 Sept 2012.

[9] Wu, B. "High-Power Convertes and AC Drivers", *The Institute of Electrical and Electronics Engineering,* 2006.

[10] M. H. Rashid, "Power Electronics Handbook", *Academic Press,* New York, 2001.

[11] Wang, C., Nehrir, M., H., Shaw, S.R., "Dynamic Models and Model Validation for PEM Fuel Cells Using Electrical Circuits", *IEEE Trans. on Energy Conversion,* Vol. 20, No. 2, pp. 442-451, 2005.

Circularly Polarized Slot Antenna for wireless Applications

Yasin AMANI[1]
Yashar ZEHFOROOSH[2]

Abstract
This letter presents a new design for a circularly polarized square slot antenna with an enhanced impedance bandwidth. The antenna structure includes a pair of inverted-L grounded arms, around two opposite corners which can result the CP bandwidth of the proposed antenna at 5.14-7.78 GHz .The designed Circularly Polarized Slot Antenna with size 25 mm (length) ×25mm (width) ×0.8 mm (height) is greatly improved for achieving a significantly enhanced impedance bandwidth of 2–13 GHz with VSWR $\leq$ 2. The simulation results have been showed that using inverted-L grounded arms , circular and strip patches are increasing the CP bandwidth and reduce the size of the proposed antenna .

Keywords: *Slot Antenna, Circular Polarization, Wireless Applications*

1. Introduction

In the past few years, the rapid development of the use of wireless and fast communications an Ultra wide band antenna such as circular polarized square a lot antenna has become an option in wireless communications systems [1]. Because of the advantages of wideband-width, low profile, uniplanar geometry, easy integration with mono- lithic microwave integrated circuits, sending and receiving without causing a polarization mismatch and overcoming the multipath fading problem, circular polarization is becoming popular [4-9]. In recent years wireless systems demand stringent physical requirements from antennas, s o different shape and type of broadband Circular polarized slot antenna have been developed to reduce the axial-ratio bandwidths (ARBWs) ,with the various design and techniques, we can achieve the right hand and the left hand CP in these kind of antenna at the same time .Some of the techniques that are used in this design are : adding two inverted-L grounded arms around two opposite corners of the antenna [1], creating inverted-L slot on the ground plane which is connected the two inverted arms together, adding a semicircular –shaped and semi stair-shape on the feed line and inverted-L grounded strips [2-3]. In addition by changing the shape of the feed line such as using arc-shape , lightning-shape , cross-shape , crane-shaped we can achieve good CP radiation characteristics for the slot antenna [1-3].

[1]*Department of Electrical Engineering, Urmia Branch, Islamic Azad University, Urmia , Iran*
[1]*Department of Electrical Engineering, Urmia Branch, Islamic Azad University, Urmia , Iran*

This novel presents an Ultra wideband circular polarized slot square antenna (CPSSA), which is used a T-shape grounded metallic strip perpendicular to the axial direction of the coplanar waveguide (CPW) feed line and semicircular and semi steps feed line to reveal the circularly polarized (CP).

2. Antenna Configuration and design

Fig. 1 illustrates the evolution of the proposed single-layer CPW-fed CPSS antenna. As shown, in fig. 1, antennas is printed on a commercially cheap FR4 substrate with a loss tangent of 0.024, permittivity of 4.4 and tiny dimensions of 25 mm (length) ×25mm (width) × 0.8 mm (thickness).As it is indicated in the figure, Two main features have been incorporated within the design: one mainly for enhancing the impedance bandwidth, and the other for enlarging the ARBW, which are reached at the proposed antenna by a tuning circle stub embedded in the feeding structure and a semi-strip main patch stuck to the feed line**.** Two inverted-L grounded arms strips are loaded in the two opposite corner of the antenna, the size of the inverted-L-shaped slot which is connected the two inverted-L-shaped strips around together is modified for having the best result .It should be noted that all units are in millimeter(mm).

The width and length of the waveguide (CPW) feed-line are 3.1 mm and 12 mm, respectively the feed line is terminated with a standard SMA connector, and to achieve 50Ω characteristic impedance the width of the gap between the feed-line and the ground plane is 0.25 mm. Furthermore, the sizes of the inverted-L- shaped strips are L17=5mm and L4=6mm. other parameters of the antenna can be found in Tab. 1

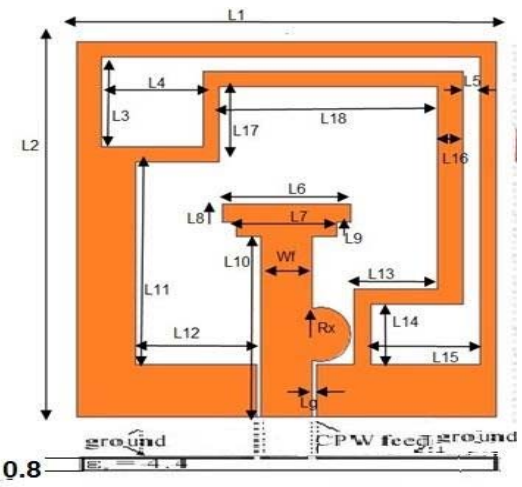

Fig. 1 Geometry of proposed CPW-fed CPSSA (all dimensions are in mm)

Table1: The dimension of the antenna parameters

Rx	1.8
Wf	3.1
Lg	0.25
L1	25
L2	25
L3	6
L4	6
L5	1
L6	7.6
L7	6
L8	1.3
L9	1
L10	12
L11	7.2
L12	13.5
L13	5
L14	4
L15	6.5
L16	1.5
L17	5
L18	13

There are three steps to release CPW-fed CP slot antenna: At the first step, embedded only a single strip and ground plane, then adding two inverted-L grounded arms strips to opposite corners and a metal semicircle to feed-line and for the third step, embedding semi-strip shaped main patch and a L-shape slot which connected the two inverted L-shaped strips together. Fig.2.a depicts the three mentioned steps of the design of the proposed antenna and Fig.2.b shows the VSWR curves of the antenna at the three designing steps with the measurement VSWR results. The simulation results show that embedding a semicircle and semi-strip shaped to the feed-line increases the impedance band-width however, the combination of the feed-line with a semicircle and semi-strip shaped patch and the inverted-L strips that lead to expanding the CP bandwidth which is mostly depends on the inverted-L-shaped stripsaround the corners of the antenna so by adding a inverted-L-shaped slot CP bandwidth be widen.

Finally the measured radiation pattern of the offered antenna will be discussed in next section.

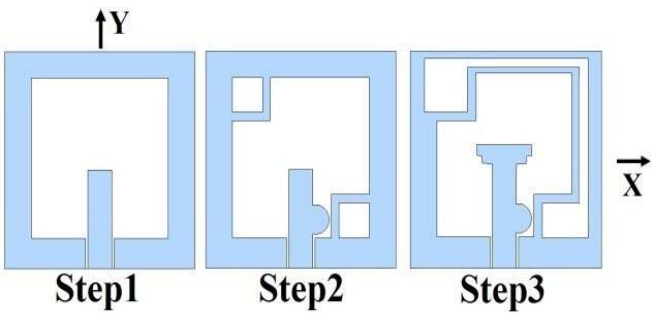

(a)

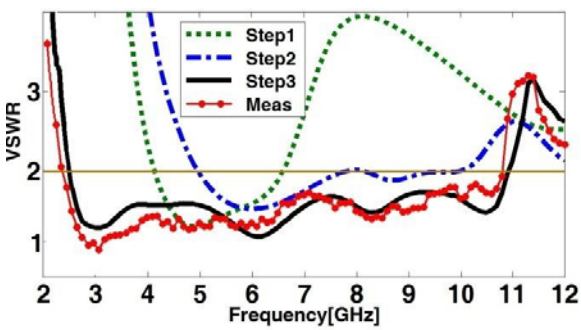

(b)

Fig.2 antenna three designing steps with VSWR results
a) Antenna three designing steps
b) VSWR curves of the antenna three designing steps and measurement VSWR results.

3. Results and Discussion

The performances of the CPSS antenna in parametric studies have been investigated to find optimized parameters using commercial Ansoft by the High Frequency Structure Simulator(HFSS13) software. The impedance bandwidth and axial ratio of the CPSSA are measured using the Agilent 8722ES network analyzer.

According the results of the numerical analysis, The optimized parameters of the proposed antenna is shown is table. 1. The simulated S11 curves for two various CPSSA parameters, Rx and L6 (radius of circle and length of the semi-strip center position, respectively) are plotted in Fig.3 and the results of the measured and simulation of the return loss of the antenna shown in the Fig4 .The measured impedance bandwidths are from 2 to 13 GHz. The result of the simulation and measured of the axial ratio showed in the Fig 6 and the RHCP and LHCP of the presented antenna shown in the Fig 7.According to the Fig.2 impedance bandwidth increase at the step 3and there is a similarity between measurement and simulation of VSWR results.

Fig.4 shows the measurement and simulation results of return loss of the proposed antenna. Our parametric simulations indicate that the radius and position of the tuning stub has important effect on the improvement of the impedance BW. From the numerical results in Fig. 3.a, it is obtained that the impedance bandwidth is expanded at the as Rx increases from 1.6mm to 1.8mm, meanwhile broader impedance BW is obtained by increasing the length of L_6 parameter, the antenna's main parameter and the size of the antenna will increase so for having a good results with reasonable size L_6=7.6 mm is selected.

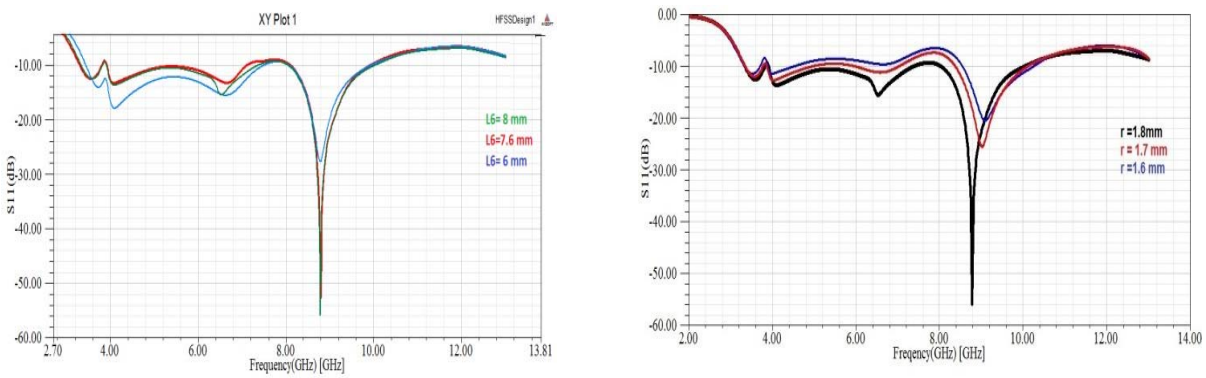

(a) (b)

Fig. 3 S11 of various value of Rx (radius of circle and length of L6)
a) S11 curves of different values of Rx
b) S11 curves of different values of L6

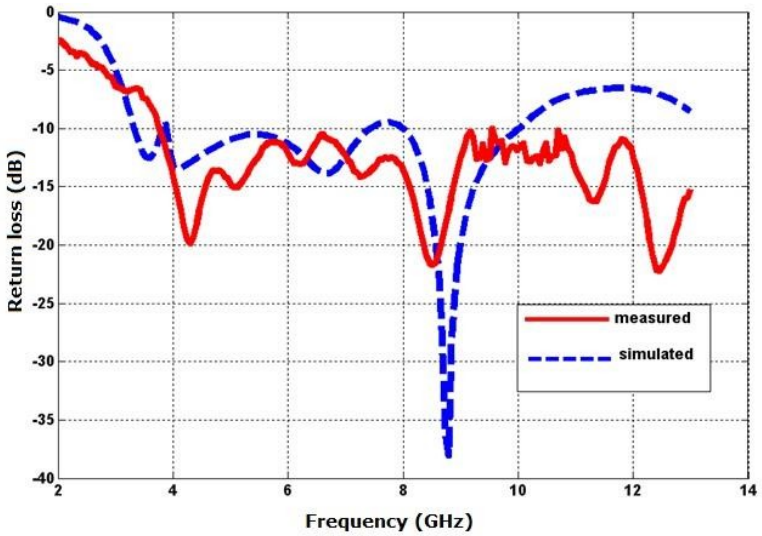

Fig.4 measured and simulated curves of Return loss

As we see in the Fig. 4 there is a good accommodation between the antenna return loss measured and analysis.

The simulated and measured gains and AR curves, depicted in Fig.5 indicates the close correspondence between the measured and simulated curves of gain and AR for the proposed antenna with optimized values presented in Fig.1 and in Table1. As plotted in Fig.6, the ARBW of the proposed antenna is from 5050 MHz to 8200 MHz (47.5%) and the obtained gain is acceptable.

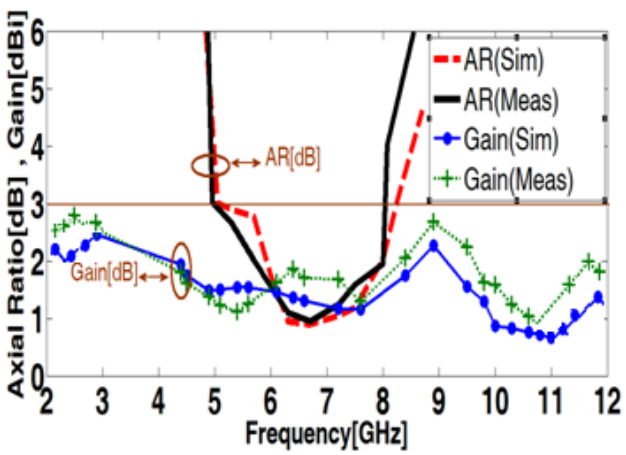

Fig.5 Measured and simulated CP axial ratios and gain of the proposed antenna

Fig.6 shows the simulated normalized RHCP and LHCP radiation patterns of the offered CPSSA at 5.5 GHz and 7.3 GHz.
Fig.7shown the simulation results of surface current distribution for the presented antenna.

As we can see the surface distribution in phase of 0° and 90° are equal in magnitude and opposite in phase 180° and 270°. The antenna right/left hand circular polarization (RCHP/LHCP) happened when the current rotates in the clockwise or counter clockwise direction. The proposed is shown at Fig. 8.

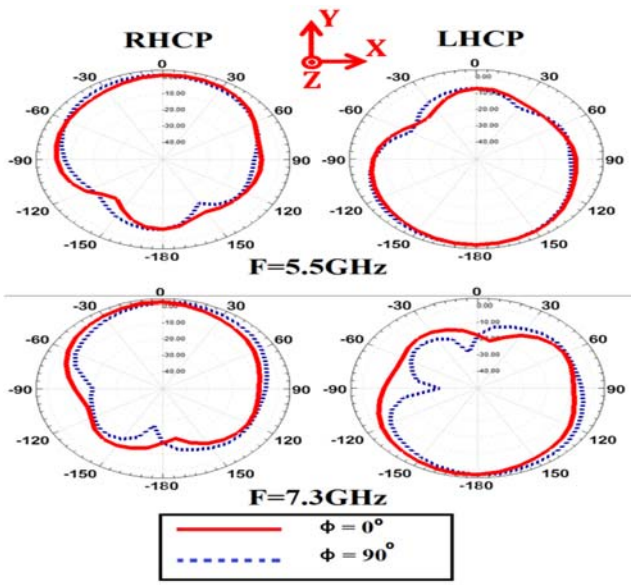

Fig. 6 Simulated radiation patterns of the proposed antenna at 5.5GHz and 7.3GHz

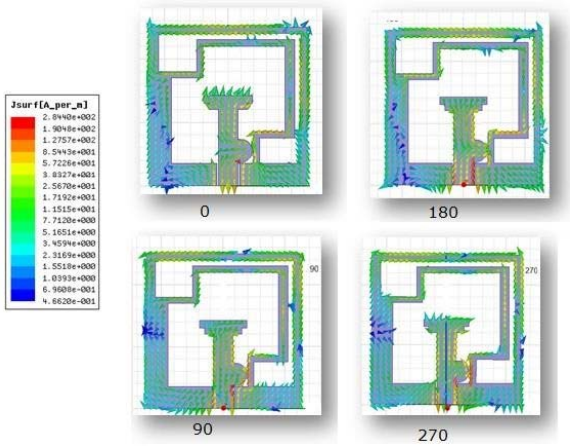

Fig. 7 Distribution of the surface current of the proposed antenna

Fig. 8. Photograph of the antenna

4. Conclusions

An Ultra-width band circular polarized square slot antenna with the CPW-fed was designed and successfully implemented. Results show that using reverse L-shaped ground arms and L-shaped notch can significantly enhance the antenna's 3 dB ARBW.

According to the results of the gain level, radiation patterns, current distributions and measured result this antenna is a good candidate for wireless and WLAN applications.

REFERENCES

[1] Javad Pourahmadazar, Ch. Ghobadi, J. Nourinia, Nader Felegari, and Hamed Shirzad, Broadband CPW-Fed Circularly Polarized Square Slot Antenna with Inverted-L Strips for UWB Applications. IEEE Antenna Wireless Propag. Lett., vol. 10, pp. 369—372, 2011.

[2] Jia-Yi sze, C-I. G. Hsu, Z-W.Chen, and C-C Chang, Broadband CPW-fed circularly polarized square slot antenna whit lightening shaped feed line and inverted-L grounded strips. IEEE Trans Antenna Propag., vol. 58, no .3, pp. 973—977, Mar. 2010.

[3] M.-J. Chiang ,T.-F. Hung, and S.-S. Bor.,―Dual-band circular slot antenna design for circularly and linearly polarized operations,‖ Microw.Opt. Technol. Lett., vol. 52, no. 12, pp. 2717–2721, Dec. 2010.

[4] Badamchi, Z. and Zehforoosh, Y. (2015), Switchable single/dual band filtering UWB antenna using parasitic element and T-shaped stub wave cancellers. Microw. Opt. Technol. Lett., 57: 2946–2950.

[5] Sefidi, M., Zehforoosh, Y. and Moradi, S. (2015), A novel CPW-fed antenna with dual band-notched charectrestics for UWB applications.

Microw. Opt. Technol. Lett., 57: 2391–2394.

[6] Siahcheshm, A., Nourinia, J., Zehforoosh, Y. and Mohammadi, B. (2015), A compact modified triangular CPW-fed antenna with multioctave bandwidth. Microw. Opt. Technol. Lett., 57: 69–72.

[7] Beigi, P., Nourinia, J., Zehforoosh, Y. and Mohammadi, B. (2015), A compact novel CPW-fed antenna with square spiral-patch for multiband applications. Microw. Opt. Technol. Lett., 57: 111–115.

[8] Zehforoosh, Y. and Sedghi, T. (2014), A CPW-fed printed antenna with band-notched function using an M-shaped slot. Microw. Opt. Technol. Lett., 56: 1088–1092.

[9] Hadi Baghali, Yashar Zehforoosh, Javad Nourinia, NOVEL SUPER WIDE BAND ANTENNA WITH WLAN/WiMAX BAND REJECTION AND COMPACT SIZE,International Journal of Electronics, Mechanical and Mechatronics EngineeringVol.3 Num 3 pp.621-624

INTERNATIONAL JOURNAL OF ELECTRONICS, MECHANICAL AND MECHATRONICS ENGINEERING

SUBMISSION INSTRUCTIONS

The scope of International Journal of Electronics, Mechanical and Mechatronics Engineering (IJEMME) covers the novel scientific papers about Electronics, Image Processing, Information Theory, Electrical Systems, Power Electronics, Control Theory, Embedded Systems, Robotics, Motion Control, Stochastic Modeling, System Design, Multidisciplinary Engineering, Computer Engineering, Optical Engineering, Design Optimization, Material Science, Metamaterials, Heat and Mass Transfer, Kinematics, Dynamics, Thermo-Dynamics, Energy and Applications, Renewable Energy, Environmental Impacts, Structural Analysis, Fluid Dynamics and related topics of the above subjects.

IJEMME is an international periodical published triple a year (February, July and October). Manuscripts reporting on original theoretical and/or experimental work and tutorial expositions of permanent reference value are welcome. IJEMME Editorial Board is authorized to accept/reject the manuscripts based on the evaluation of international experts. The papers should be written in English.
The manuscript should be sent in electronic submission via **zaferutlu@aydin.edu.tr**

SUBMISSION INSTRUCTIONS OF MANUSCRIPTS.

Page Design: Text body area is (195mm x 275mm). 30 mm margin from top, 20 mm from down and 25 mm margin should be left on right/left sides.

Title: should be in 16 pt. bold, capital letters with Times New Roman font in Microsoft Word format. Authors' names, affiliations, e-mail addresses should follow the title after double line spacing with authors' names and surnames in lower case except first letters in 14 pt, the rest is 10 pt. italic.

Abstract: should not exceed 200 words with the word "Abstract" in 10 pt. italic, bold, abstract text in 9 pt. italic, all in Times New Roman font in Microsoft Word format.

Keywords: not exceeding 5 should be in bold.

Document Character: Subtitles should be in 10 pt. bold, capital letters and text body 10 pt. both with Times New Roman font in Microsoft Word format. The manuscripts should be written on a single column, be double spaced with single line spacing between paragraphs. The subtitle of the first section should start after a single space following the keywords, the other subtitles also with a single line space following the text, there should also be single line spacing between the previous text and the subtitle.

CONCLUSION section should have a title written in 1o pt. bold, capital letters and the text in 10 pt. all in Times New Roman font in Microsoft Word format.
REFERENCE numbers should be given in brackets as illustrated below:
Referencing books:

[1] Özsu M., T, Valduriez, P., Principles of Distributed Database Systems, Prentice Hall, New Jersey, 128-136,1991.

Referencing papers:

[2] G. Altay, O. N., Ucan, "Heuristic Construction of High-Rate Linear Block Codes," International Journal of Electronics and Communications (AEU), vol. 60, pp.663-666, 2006.

Page number is to be placed at the top left corner of each page with pencil.
Length of the Manuscript should not exceed 20 pages excluding Figures and Tables.

INSTRUCTIONS ABOUT THE ACCEPTED MANUSCRIPTS:

Page Design: Text body area is (195mm x 275mm). 30 mm margin from top, 20 mm from down and 25 mm margins should be left on right/left sides.

Title: should be in 16 pt. bold, capital letters with Times New Roman font in Microsoft Word format. Authors' names, affiliations, e-mail addresses should follow the title after double line spacing with authors' names in lower case and surnames in capital letter in 14 pt. the rest in 10 pt. in the same format.

Abstract: should not exceed 200 words with the word "Abstract" in 12 pt. italic, bold, abstract text in 9 pt. italic, all in Times New Roman font in Microsoft Word format.

Keywords: not exceeding 5 should be in 9 pt. bold.

Document Character: Subtitles should be in 10 pt. bold, capital letters and text body 10 pt. both with Times New Roman font in Microsoft Word format. **The manuscripts should be written on two columns, be single spaced with single line spacing between paragraphs.** The subtitle of the first section should start after a single space following the keywords, the other subtitles also with a single line space following the text, there should also be single line spacing between the previous text and the subtitle.

SECTIONS: Formulas should be numbered sequentially. Referring to formulas should be as Eqn (.). Figures and Tables should be placed into the text body and captions for both should be 10 pt. Table numbers and captions should be placed before the Table. If necessary, both columns may be used for large Figures and Tables.

CONCLUSION section should have a title written in 12 pt. bold, capital letters and the text in 10 pt. all in Times New Roman font in Microsoft Word format. Conclusion should not be a version of the Abstract.
REFERENCE numbers should be given in brackets as illustrated below:

Referencing books:
[1] Özsu M., T, Valduriez, P., Principles of Distributed Database Systems, Prentice Hall, New Jersey, 128-136,1991.

Referencing papers:

[2]G. Altay, O. N., Ucan, "Heuristic Construction of High-Rate Linear Block Codes," International Journal of Electronics and Communications (AEU), vol. 60, pp.663-666, 2006.

SHORT BIOGRAPHY of the authors should follow references after a single line space, names in 9 pt. surnames in 9 pt. and the text in 9 pt. The text should not exceed 100 words.

CORRESPONDENCE ADDRESS:

Editor
Prof. Dr. Zafer UTLU
Engineering Faculty
Mechanical Engineering Department
Inonu Caddesi, No.38, Florya, Istanbul, TURKEY
E-mail: zaferutlu@aydin.edu.tr
Web : www.aydin.edu.tr/eng/ijemme

Prepared by
Instructor: Şenay KOCAKOYUN
Anadolu BIL Vocational High School
Computer Programming Department
Inonu Caddesi, No.38 Florya, Istanbul, TURKEY
E-mail: senaykocakoyun@aydin.edu.tr

Published by
Istanbul Aydın University